

**TRANSPARENT ELECTRODE FOR  
HARVESTING ENERGY USING A  
THERMOELECTRIC PRINCIPLE**

**TAI ZHEN HANG**

**UNIVERSITI TUNKU ABDUL RAHMAN**

**TRANSPARENT ELECTRODE FOR HARVESTING ENERGY USING  
A THERMOELECTRIC PRINCIPLE**

**TAI ZHEN HANG**

**A project report submitted in partial fulfilment of the  
requirements for the award of Bachelor of Engineering  
(Honours) Mechatronics Engineering**

**Lee Kong Chian Faculty of Engineering and Science  
Universiti Tunku Abdul Rahman**

**October 2022**

**DECLARATION**

I hereby declare that this project report is based on my original work except for citations and quotations which have been duly acknowledged. I also declare that it has not been previously and concurrently submitted for any other degree or award at UTAR or other institutions.

Signature :  \_\_\_\_\_

Name : Tai Zhen Hang \_\_\_\_\_

ID No. : 18UEB06667 \_\_\_\_\_

Date : 2 October 2022 \_\_\_\_\_

**APPROVAL FOR SUBMISSION**

I certify that this project report entitled “**TRANSPARENT ELECTRODE FOR HARVESTING ENERGY USING A THERMOELECTRIC PRINCIPLE**” was prepared by **TAI ZHEN HANG** has met the required standard for submission in partial fulfilment of the requirements for the award of Bachelor of Engineering (Honours) Mechatronics Engineering at Universiti Tunku Abdul Rahman.

Approved by,

Signature :  \_\_\_\_\_

Supervisor : Ir. Dr. Chee Pei Song

Date : 2 October 2022

Signature : \_\_\_\_\_

Co-Supervisor : \_\_\_\_\_

Date : \_\_\_\_\_

The copyright of this report belongs to the author under the terms of the copyright Act 1987 as qualified by Intellectual Property Policy of Universiti Tunku Abdul Rahman. Due acknowledgement shall always be made of the use of any material contained in, or derived from, this report.

© 2022, Tai Zhen Hang. All right reserved.

## **ACKNOWLEDGEMENTS**

I would like to thank everyone who had contributed to the successful completion of this project. I would like to express my gratitude to my research supervisor, Ir. Dr. Chee Pei Song for his invaluable advice, guidance and his enormous patience throughout the development of the research.

In addition, I would also like to express my gratitude to my loving parents and friends who had helped and given me encouragement especially Vinod A/L N. Rajandran for his continuous support.

## ABSTRACT

Everyone relies on electricity to power up electronic gadgets, lights, medical equipment, commute between cities and countless others. Nevertheless, electricity is primarily produced by burning fossil fuels or other non-renewable sources which resulted in many unfavourable consequences such as pollutions, global warming, and climate change. One of the recent developments focus on generating electricity directly from heat, exploiting Seebeck effect. Transparent thermoelectric generator (t-TEG) is a transparent device that can generate electricity when subjected to a temperature gradient across it. It not only serves in power generating applications but also in imperceptible robotics, sensors, advanced materials and wearables. In this research project, a number of t-TEGs were fabricated by spin-coating and direct deposition methods under UTAR Sungai Long Campus laboratory setting. The selected p-type material was PEDOT:PSS and n-type material was ITO. The highest output power of the t-TEG ( $0.0006 \text{ m}^2$ ) was recorded at 32.58 nW when subjected to a temperature gradient of  $120 \text{ }^\circ\text{C}$ . This t-TEG had 5 layers of PEDOT:PSS thin films coated on a glass substrate and exhibited an average % transmittance above 80 %. As compared to the similar work reported by Wang et al., their t-TEG had a power density of  $22.2 \text{ Wm}^{-2}$  which was significantly higher than the t-TEG fabricated in this project. This was mainly because they utilized trifluoromethanesulfonic-methanol mixture, TFMS-MeOH (V:V = 1:10) chemical to treat the PEDOT:PSS prior to pairing with ITO and they connected 10 pairs of these thermocouples in series. By purchasing TFMS-MeOH to post-treat PEDOT:PSS and improve morphology of the t-TEG in further study, a greater output power is possible.

## TABLE OF CONTENTS

<b>DECLARATION</b>		<b>i</b>
<b>APPROVAL FOR SUBMISSION</b>		<b>ii</b>
<b>ACKNOWLEDGEMENTS</b>		<b>iv</b>
<b>ABSTRACT</b>		<b>v</b>
<b>TABLE OF CONTENTS</b>		<b>vi</b>
<b>LIST OF TABLES</b>		<b>ix</b>
<b>LIST OF FIGURES</b>		<b>x</b>
<b>LIST OF SYMBOLS / ABBREVIATIONS</b>		<b>xiii</b>
<b>LIST OF APPENDICES</b>		<b>xiv</b>
<b>CHAPTER</b>		
<b>1</b>	<b>INTRODUCTION</b>	<b>1</b>
1.1	General Introduction	1
1.2	Importance of the Study	3
1.3	Problem Statement	3
1.4	Aim and Objectives	4
1.4.1	Aim	4
1.4.2	Objectives	4
1.5	Scope and Limitation of the Study	4
1.6	Contribution of the Study	5
1.7	Outline of the Report	5
<b>2</b>	<b>LITERATURE REVIEW</b>	<b>6</b>
2.1	Introduction	6
2.2	Emergence of Green and Renewable Energy	6
2.3	Photovoltaic Solar Energy and Its Limitations	7
2.4	Thermoelectric Energy	8
2.5	Thermoelectric Generator Basic Structure	9
2.6	Selection of Thermoelectric Materials	10
2.7	Nanostructured Thermoelectric Materials	12

2.8	Transparent Thermoelectric Generator	13
2.9	Transparency of a Material	14
2.10	Examples from Other Researchers	15
2.11	Summary	20
<b>3</b>	<b>METHODOLOGY AND WORK PLAN</b>	<b>21</b>
3.1	Introduction	21
	3.1.1 Introduction to Spin Coating Method	21
	3.1.2 Introduction to Corona Treatment	23
3.2	Locations, Equipment and Materials	24
3.3	Cost	27
3.4	Transparent Thermoelectric Generator Fabrication	28
	3.4.1 Procedure to Make Transparent Thermoelectric Generator	29
	3.4.2 Precaution	33
3.5	CJMCU-3108 Ultra-low Voltage Booster Set Up	35
	3.5.1 Procedure to Set Up CJMCU-3108 Ultra- low Voltage Booster	35
3.6	Summary	39
<b>4</b>	<b>RESULTS AND DISCUSSION</b>	<b>40</b>
4.1	Introduction	40
4.2	Output Voltage and Output Current of TEGs with PEDOT:PSS Spin-Coated	41
4.3	Output Voltage and Output Current of TEGs with Non-spin-coated PEDOT:PSS	46
4.4	TEGs with Non-spin-coated PEDOT:PSS Connected in Series	51
4.5	TEGs with Non-spin-coated PEDOT:PSS Connected in Parallel	54
4.6	Output Power of All TEGs	58
4.7	Accuracy of Keithley 6514 System Electrometer	60
4.8	Transparency of PEDOT:PSS Thin Layers	63
4.9	Effect of High Temperature on the Transparency of t-TEGs	65

		viii
	4.10 Summary	67
<b>5</b>	<b>CONCLUSIONS AND RECOMMENDATIONS</b>	<b>68</b>
	5.1 Conclusions	68
	5.2 Recommendations for Future Work	68
	<b>REFERENCES</b>	<b>69</b>
	<b>APPENDICES</b>	<b>76</b>

## LIST OF TABLES

Table 2.1:	TEG Modules Reported by Other Researchers and Their Respective Parameters.	19
Table 3.1:	Locations and Their Services Provided.	24
Table 3.2:	Equipment and Materials.	25
Table 3.3:	Items Purchase and Their Price.	27
Table 3.4:	Five Samples with Their Respective Number of PEDOT:PSS Layers.	30
Table 3.5:	Transparency of Glass Substrate with Different PEDOT:PSS Layers	38
Table 4.1:	Output Voltage of a Single TEG with Different PEDOT:PSS Layer(s).	42
Table 4.2:	Output Current of a Single TEG of Different PEDOT:PSS layer(s).	44
Table 4.3:	Output Voltage of a TEG (PEDOT:PSS Non-spin-coated).	47
Table 4.4:	Output current of a single TEG (PEDOT:PSS non-spin-coated).	49
Table 4.5:	Output Voltage and Output Current of Five TEGs and Nine TEGs, Both Connected in Series and PEDOT:PSS Non-spin-coated.	52
Table 4.6:	Output Voltage and Output Current of Five TEGs in parallel.	55
Table 4.7:	Average Output Power of all TEGs.	58
Table 4.8:	Rising Hotplate Temperature Only Resulted in Negligibly Small Voltage Reading on The Electrometer.	61
Table 4.9:	Transparency of Glass Substrate with Different PEDOT:PSS Layers.	63
Table 4.10:	Discoloration of Clear Epoxy After Exposure to High Temperature.	66

## LIST OF FIGURES

Figure 2.1:	Basic Structure of a Thermoelectric Generator.	9
Figure 2.2:	The Relationship between Carrier Concentration of a Thermoelectric Material and the ZT Value Together with Other Thermoelectric Parameters. Reprinted from Materials Science in Semiconductor Processing, 121/105303, Ma et al., Review of Experimental Approaches for Improving ZT of Thermoelectric Materials, Copyright 2021, with Permission from Elsevier.	11
Figure 2.3:	Structure of GTO Thermoelectric Generator Proposed by Yamamoto et al. (2021) and Kimura et al. (2022).	16
Figure 3.1:	Schematic Diagram of a Spin Coater. Reprinted from Current Trends and Future Developments on (Bio-) Membranes: Photocatalytic Membranes and Photocatalytic Membrane Reactors, (Chen et al., 2018), Materials and Design of Photocatalytic Membranes, pg. 71-96, Copyright 2018, with Permission from Elsevier.	22
Figure 3.2:	Four Main Components of the Handheld Corona Treater.	23
Figure 3.3:	Corona Treatment on Glass Substrate.	29
Figure 3.4:	70 $\mu$ L PEDOT:PSS Solution on Glass Substrate.	30
Figure 3.5:	Final Prototype.	31
Figure 3.6:	K6514 Application Homepage.	32
Figure 3.7:	Avoid Excessive Force When Cutting Glass Substrate.	33
Figure 3.8:	Maximum Safe Sash Height.	33
Figure 3.9:	Example of an Experimental Set Up.	34
Figure 3.10:	Reset Button.	34
Figure 3.11:	Soldering Transformer into Breakout Board.	35
Figure 3.12:	Soldering Pin Header onto Breakout Board.	36
Figure 3.13:	Circuit Diagram to Connect Pins on the CJMCU-3108 Breakout Board.	37

Figure 3.14:	Actual Wire Connection of the CJMCU-3108 Breakout Board.	38
Figure 4.1:	Experimental Setup to Characterize TEG (PEDOT:PSS Spin-coated).	41
Figure 4.2:	Output Voltage vs Temperature Gradient (1 Layer PEDOT:PSS).	43
Figure 4.3:	Output Voltage vs Temperature Gradient (3 Layers PEDOT:PSS).	43
Figure 4.4:	Output Voltage vs Temperature Gradient (5 Layers PEDOT:PSS).	43
Figure 4.5:	Output Current vs Temperature Gradient (1 Layer PEDOT:PSS).	45
Figure 4.6:	Output Current vs Temperature Gradient (3 Layers PEDOT:PSS).	45
Figure 4.7:	Output Current vs Temperature Gradient (5 Layers PEDOT:PSS).	45
Figure 4.8:	Experimental Setup to Characterize TEG (PEDOT:PSS Non-spin-coated).	46
Figure 4.9:	Output Voltage vs Temperature Gradient (PEDOT:PSS Non-spin-coated).	48
Figure 4.10:	Output Current vs Temperature Gradient (PEDOT:PSS Non-spin-coated).	50
Figure 4.11:	Five TEGs Connected in Series (Left) and Nine TEGs Connected in Series (Right).	51
Figure 4.12:	Outputs of Five TEGs in Series vs Nine TEGs in Series (PEDOT:PSS Non-spin-coated).	53
Figure 4.13:	Five TEGs Connected in Parallel.	54
Figure 4.14:	Output Voltage of Five TEGs in Parallel (PEDOT:PSS Non-spin-coated)	56
Figure 4.15:	Output Current of Five TEGs in Parallel (PEDOT:PSS Non-spin-coated)	57
Figure 4.16:	Both Positive Probe and Negative Probe Were Placed Approximately 10 mm Above the Hotplate Which Temperature Rose from 26 °C to 176 °C.	60

Figure 4.17: Electrometer Voltage Reading vs Hotplate Temperature.	62
Figure 4.18: Electrometer Current Reading vs Hotplate Temperature.	62
Figure 4.19: % Transmittance of Glass Substrate and Glass Substrate with Different Layers of PEDOT:PSS.	64
Figure 4.20: Some Samples of Fabricated TEGs.	67

**LIST OF SYMBOLS / ABBREVIATIONS**

$S^2\sigma$	Electron power factor, $W \cdot m^{-1} \cdot K^{-2}$
$ZT$	Figure of merit
$S$	Seebeck coefficient, $VK^{-1}$
$T$	Absolute temperature, K
$\kappa$	Thermal conductivity, $W \cdot m^{-1} \cdot K^{-1}$
$\kappa_L$	Lattice thermal conductivity, $W \cdot m^{-1} \cdot K^{-1}$
$\sigma$	Electrical conductivity, $S \cdot cm^{-1}$
AgNWs	Silver nanowires
CNT	Carbon nanotube
CVD	Chemical vapor deposition
DCL	Department of Chemical Engineering
DMBE	Department of Mechatronic & Biomedical Engineering
DMME	Department of Mechanical and Material Engineering
f-TEG	Flexible thermoelectric generator
IoT	Internet of things
ISR	Imperceptible soft robotics
ITO	indium tin oxide ( $In_2O_5Sn$ )
LED	Light-emitting diode
MWCNT	Multi-walled carbon nanotube
OSC	Organic solar cell
PCE	Power conversion efficiency
PEDOT:PSS	Poly(3,4-ethylenedioxythiophene) polystyrene sulfonate
PEI	Polyethylenimine
RF	Radio frequency
STO	Strontium titanate (STO)
t-TEG	Transparent thermoelectric generator
TEG	Thermoelectric generator
TFMS	Trifluoromethanesulfonic ( $CF_3SO_3H$ )
TFMS	Trifluoromethanesulfonic acid ( $CF_3SO_3H$ )
VSSA	Volume specific surface area
XRD	X-ray diffraction

**LIST OF APPENDICES**

Appendix A: Gantt Chart for January 2022 Trimester	76
Appendix B: Gantt Chart for May 2022 Trimester	77

## CHAPTER 1

### INTRODUCTION

#### 1.1 General Introduction

Electrical power is an essential energy in human's daily life. It powered up all sorts of the lighting, computers, mobile gadgets, medical devices, manufacturing process, communication facilities, satellite, and countless other electronic and electrical appliances. According to U.S. Energy Information Administration (2021), there are various means to generate electrical power such as by turning conventional steam / combustion turbine (i.e., burning of coal, natural gas, and biomass) (62.1%), wind turbine (8.4%), hydroelectric turbine (7.1%), photovoltaic cells (2.1%), and others. Particularly, Malaysia generated a total electrical power of 175 996 GWh in year 2019. 84% of this total electrical power produced was dominated by burning fossil fuels such as oil, natural gas, and coal (International Renewable Energy Agency, 2021). In fact, converting energy from fossil fuels to electrical power began as early as the industrial revolution took place in 1760s (Ritchie, Roser and Rosado, 2020). It has been a common electricity-generating practice accepted worldwide. Nonetheless, burning fossil fuel emits hazardous greenhouse gases which are the main drivers of climate change and pollution. Some examples of greenhouse gases are nitrogen oxides, carbon dioxide, and methane. Nitrogen oxides is the main culprit of acid rain, imbalanced aquatic ecosystem, and smog (U.S. Environmental Protection Agency, 2022) while carbon dioxide and methane gases are responsible for global warming as it shreds the ozone layer and traps heat within earth atmosphere, respectively (Denchak, 2018; Mcsweeney, 2020). Moreover, degradation of air quality also directly jeopardizes one's health conditions by increasing the likelihood of development cardiovascular disease and respiratory illnesses (National Institute of Environmental Health Sciences, 2022).

Thankfully, there are counterefforts to gradually replace these non-renewable energies with other more environment friendly sources such as hydroelectric energy, wind energy, and solar energy (Morse, 2013). According to Malaysian Investment Development Authority (2022), Malaysian

government is prioritizing the implementation of solar energy projects due to the lower cost of photovoltaic technologies and hardware. The government also provides attractive financing services to investors to upscale the solar energy utilization and even had approved 1162 solar energy projects in 2020 which worth RM348.8 billion. Nevertheless, the state-of-the-art solar cell technology has a capped energy conversion efficiency of 47.1% (Geisz et al., 2020). The efficiency drops to only around 20% for most commercial solar cells and it posted some limitations such as large land-area occupation and vulnerable to high surrounding temperature. Its limitations are discussed in more details at the literature review section.

On the other hand, using heat (thermal energy) to generate electricity has been an area of interest for decades. When two different conducting materials are connected and one of its ends is heated to a temperature higher than the other end, a voltage difference across these two ends can be observed. This phenomenon is known as Seebeck effect. Not all materials exhibit this attribute and for materials which show this property are referred as thermocouples. This special phenomenon ignites a novel thought of harvesting thermal energy from sunlight or surrounding of higher temperature and transform it to the most sought-after electrical energy. This idea is especially practical in urban area where land is scarce and crowded by high-rise buildings. According to a research authored by Jamaludin et al. (2015), the temperature difference between outdoor and indoor could reach 6 °C in typical Malaysia daytime. This indoor-outdoor temperature difference easily doubles if indoor air conditioner is switched on. Also, it has high possibility to be exploited to generate electricity using Seebeck effect. The next doubt pops up when it comes to choosing the appropriate places to install the thermoelectric generator (TEG) within a building. Window seems to be the suitable place since it is more accessible, and it allows the TEG to be installed onto existing buildings as a separated gadget without altering the buildings' concrete structures.

However, conventional and commercially available TEGs are opaque. They block sight and affect indoor natural illumination if they are installed onto window. Therefore, transparent TEG is needed but it is still in research and development stage. There are limited known transparent materials that can

be paired as thermocouples and their output powers are usually minuscule. As a result, this research project aims to explore various materials that could be paired as thermocouples of highest output possible and to fabricate a TEG module using this thermocouple. This endeavour not only serves as a pioneer to encourage the use of thermal energy to produce electricity but also expose a new perspective of transparent power-generating device using Seebeck effect. This will also benefit the applications of advanced materials, soft robotics, wearables, and sensors.

## **1.2 Importance of the Study**

As compared to opaque TEG, there exist few successful studies conducted by other researchers to fabricate a transparent TEG module which output is high enough to show meaningful usage such as powering up a LED. This study explores other researchers' works and take initiative to venture into this uncertain transparent TEG territory. In addition, this study introduces a novel method to harvest thermal energy from atmosphere and convert the thermal energy into electrical power. This method is especially relevant to Malaysia situation because its weather is consistently hot throughout a year. Efforts put on this study also advocate the 7<sup>th</sup> and 13<sup>th</sup> Sustainable Development Goals which are “affordable and clean energy” and “climate action”, respectively. The procedure of making a transparent TEG module in this report can also serve as a guideline for other researchers or hobbyists. It promotes the importance and adoption of renewable energy harvesting in the context of Malaysia public awareness as well as the government's ambition to hit 31% renewable energy capacity by 2025 (Malaysia Investment Development Authority, 2021). Moreover, transparent TEG can also expand the border of imperceptible soft robotics and thermocouple sensor.

## **1.3 Problem Statement**

Burning fossil fuel to generate electricity has posed many side effects such as pollution, climate crisis and health issues. Besides existing renewable energies, thermal energy appears to be abundant and easily harvested through thermoelectric principle. Conventional thermoelectric generator has high energy conversion efficiency but not transparent. Its opacity restrains it from

installing on window to harvest thermal energy directly from sunlight. Hence, transparent TEG is widely demanded and delicate investigations are necessary to improve its comparatively low-performance.

## **1.4 Aim and Objectives**

### **1.4.1 Aim**

To fabricate a transparent thermoelectric generator (t-TEG) and characterise its output parameters.

### **1.4.2 Objectives**

1. To determine the materials that could be paired as a thermocouple of highest output power possible.
2. To fabricate a transparent TEG module on a glass substrate using spin coating method.
3. To characterise the output parameters of the transparent TEG module using an electrometer.

## **1.5 Scope and Limitation of the Study**

The basic knowledge of thermoelectric principle and the fundamental structure of a TEG are covered in this FYP. Transparent TEGs fabricated by other researchers were referred and the one with the highest output power was reproduced and synthesized. All the experiments and testing were carried out in KB615 and KB725 laboratory. The TEG module was spin-coated on a glass substrate to achieve thin-film feature and therefore transparent electrode. The thin films were made using only spin-coating method. Magnetron sputtering method, chemical vapor deposition method, spray coating method and pulse laser deposition method were not applied in this study due to lack of equipment. Only four important parameters of the TEG modules were measured, namely transparency, output voltage, output current and output power. Other mechanical and electrical properties of the transparent electrode such as the chemical state, thickness, surface smoothness, thermal conductivity, surface morphology, carrier concentration, and crystalline structure were not characterized. Many journals were using X-ray diffraction (XRD) spectra to study the crystalline structure and composition of their synthesized TEG

module. Although there was a X-ray diffractometer located in KB732, the crystalline structure of the TEG sample in this research was not analysed.

## **1.6 Contribution of the Study**

Most commercially available thermoelectric generators were opaque and did not fit into some advanced applications such as power-generating window, imperceptible robotics and wearables. In addition, t-TEGs were just being focused recently and not much research had been successfully done to improve its output voltage and output current. This research project aimed to fabricate a t-TEG under UTAR Sungai Long Campus laboratory setting and to study its output parameters. A set of PEDOT:PSS thin-films with different thickness would be paired with ITO and to observe their output parameters when subjected to a temperature gradient. The fabrication method reported in this report would also serve as a useful reference and catalyst to benefit the upcoming scholars and researchers to further enhance and broaden the functionality and output performance of t-TEG.

## **1.7 Outline of the Report**

This report first gave a brief introduction of the thermoelectric background followed by its aim and objectives. After that, it went to the literature review section where works presented by other researchers were studied and discussed. Next, it reported the methodology and fabrication-related matters in detail. A comprehensive, step-by-step experiment procedure was included in that section as well. The following section documented the experimental results and discussion of the data obtained. The last part enclosed a brief conclusion and some recommendations to be made in future work. The language and writing style used in this report was entry-level and thus suitable for a wide range of audience even for those who were not from this specialty.

## CHAPTER 2

### LITERATURE REVIEW

#### 2.1 Introduction

In this section, the importance of renewable energies was firstly discussed. Secondly, the working principle of solar photovoltaics and its limitations were briefly elaborated. Thermoelectric energy was then introduced to potentially compensate some short-comings of the present solar photovoltaics. Thirdly, the thermoelectric working principles and the basic structure of a TEG were explained. Fourthly, common materials that are used to make TEGs were explored and the ways to boost the performance of a TEG were also being investigated. Fifthly, it led to the interest of developing transparent TEG by using novel materials such as conductive polymer and thin films. Lastly, some valuable journals reporting on the fabrication of transparent TEGs were studied and referred.

#### 2.2 Emergence of Green and Renewable Energy

Global warming has been an international concern since 1850 which caused by increasingly active human activities. Among these human activities, civilization and industrialization strive to produce heat and electricity with another mean of energy source, fossil fuel (Ahmad and Zhang, 2020). Burning fossil fuel induces an unprecedented increase of temperature on the planet (Chatterjee, Chatterjee and Islam, 2022). It is mainly because the burning process releases greenhouse gases such as CO<sub>2</sub> (carbon dioxide), N<sub>2</sub>O (nitrous oxide), CH<sub>4</sub> (methane), and water vapor. According to Kuang (2021), burning fossil fuel and industrial processes contribute 65% of total CO<sub>2</sub> emission worldwide. Sunlight transmits heat onto the earth in the form of solar radiation but the greenhouse gases act as an obstacle for the heat to be dissipated out from the earth surface. This results in a cumulative amount of heat being trapped underneath the atmosphere (Mella, 2022). Besides detrimental pollution and other adverse effects, fossil fuel is a finite reserve which will deplete one day in the future (Abas, Kalair and Khan, 2015). As a result, utilization and accelerating development of renewable energies such as

biomass, geothermal heat, wind power and solar power are efforts made to mitigate the global warming issue as well as other pollution problems derived from fossil fuel consumption (Yuan et al., 2022). Most types of renewable energy applications harvest tremendous amounts of energies that naturally exist in the surrounding environment. For instances, solar power is leveraged to generate electricity using photovoltaic effect, wind's kinetic energy is harnessed by wind turbine and converted into electrical power, flowing water turns the turbine of a generator to yield hydroelectricity or hydroelectric power (Enescu, 2019a).

### **2.3 Photovoltaic Solar Energy and Its Limitations**

Among all the recognised renewable energies, solar energy poses the highest potential to be harvested in Malaysia nationwide where solar energy alone is capable to generate an estimated maximum output power of 6500 MW annually. Particularly in Malaysia, the weather is almost sunny throughout the year and solar energy projected on its land can reach up to 1900 kWh/m<sup>2</sup> (Ahmad, Kadir and Shafie, 2011). The semiconductor materials on a solar cell convert solar energy into electricity thanks to photovoltaic effect. It is more intuitive to explain photovoltaic effect using quantum theory which deems sunlight contains a bunch of energised particles, known as photons. These photons strike onto the semiconductor materials and excite its valence electrons to move more freely. The free electrons are then being directed to an external power storage system or to electrify external electrics. The free electrons eventually return to their in-situ positions, known as holes, through a hardwire connected to the solar cell. The identical process will happen again whenever a photon hits an electron, thus realizing a self-sustaining energy source (Nelson, 2003). However, the commercially available photovoltaic technology restrains the peak efficiency of a solar cell to only 13% ~ 20%. In most cases, the peak efficiency can hardly be achieved due to several reasons such as contaminated solar cell surface, cloudy weather, surrounding humidity, and temperature. The amount of sunlight is also distributed unevenly across the globe and is further subjected to sunny weather and daytime (Bagher et al., 2015). In fact, the peak efficiency is only possible when the temperature of the solar cell is stabilised at standard 25 °C. For every 1 °C increase above the

standard temperature, the efficiency will reduce by roughly 0.5 % (Elias et al., 2021).

Thankfully, the solar energy can be harvested in several ways but not only through photovoltaic conversion. One of the obvious ways is to make use of its abundant thermal energy (heat) such as hanging laundry outdoor to let it dry by the heat. This direct use of solar energy is also known as passive solar energy (Tong, Chen and Xu, 2022). On the other hand, if a mechanical device is involved to capture its thermal energy, it is then referred as solar thermal energy (Hu et al., 2021). Thermal energy comes not only from solar thermal energy but also other sources such as combustion, friction, and human body. When this thermal energy is consumed to generate electrical energy (movement of electrons), it rises a term, thermoelectric energy (Enescu, 2019). Thermoelectric energy is one of the amplest sources of renewable energy to generate electricity by absorbing heat (Yu et al., 2019). The device capable of converting thermal energy into electricity is known as thermoelectric generator (TEG). In particular, TEG aims to harvest low-temperature heat ( $<100\text{ }^{\circ}\text{C}$ ) from various origins such as sunlight (Félix-Herrán et al., 2022), furnace (Marchenko, 2020), vehicle exhaust pipe (Kim et al., 2022), and human body (Jung et al., 2022). In 1821, a German physicist, Thomas Johann Seebeck noticed an electrical potential difference when one junction of two different metals was heated (Balachander, 2019). These two different metals were thermally linked in parallel, electrically linked back-to-back (Ahmed et al., 2021). This electricity generating phenomenon induced by temperature difference across two difference materials (or known as thermocouple) is later known as Seebeck effect (Lu, 2014).

## **2.4 Thermoelectric Energy**

As compared to other renewable energies harvesting, the process of exploiting thermoelectric power introduces many advantages such as no moving parts (Zeng et al., 2022), light weight (Al-Tahaine and AlEsa, 2022), low cost (Li et al., 2022), easy maintenance (Zheng et al., 2022), and many others. Besides, the advancements in polymer and soft robotics have allured huge interests in exploring and fabricating TEG which is flexible and transparent (Zeng et al., 2022). These flexible and transparent TEGs are favourable in various

applications such as wearable medical devices (Ding et al., 2019), untethered electronic machines (Liao et al., n.d.), human-computer interface (Tan et al., 2022), and smart window (Vora-ud et al., 2022).

## 2.5 Thermoelectric Generator Basic Structure

The existing structural design of a TEG is mature and standardized. Figure 2.1 illustrates the schematic diagram of a typical TEG (Hendricks and Crane, 2012; Enescu, 2019; Jouhara et al., 2021). For a TEG to generate electricity, it must first have a pair of P-type material and N-type material. They usually appear in pillar shape and a pair of it is known as thermocouple. P-type material has extra holes (positive) which can attract electrons while N-type material has extra electrons (negative) which can freely move. When there exists a temperature gradient between two ends of a TEG, i.e. one side is hotter than the another, the electrons inside N-type materials get excited by absorbing thermal energy (heat) and tend to flow from the hot side to the cold side. Its cold side then connects to the P-type materials through an electrically conductive cold junction, commonly made out of copper (Jaziri et al., 2020). The holes (immobile) inside P-type material pave the road for the electrons to bypass it and the electrons cross the hot junctions to another N-type material. All the cumulative electrons will eventually leave the TEG to do electrical work before they return to their orbitals. For some TEGs, the ceramic plate can be replaced by polymer or silicon (Jaziri et al., 2020).

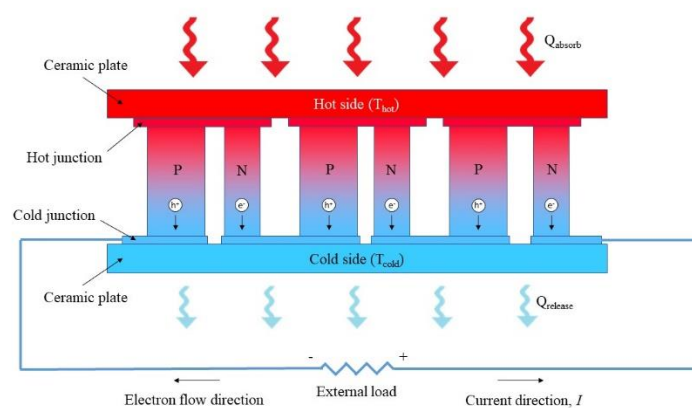


Figure 2.1: Basic Structure of a Thermoelectric Generator.

## 2.6 Selection of Thermoelectric Materials

In order to attain the desired performance of a TEG, careful selection of P-type and N-type materials plays a crucial role (Jaziri et al., 2020). Almost all literature mentioned about the thermoelectric figure-of-merit (some also refer it as dimensionless figure-of-merit). It is a key parameter to indicate how suitable a selected material can be used inside a thermoelectric device to efficiently convert heat into electrical energy and vice versa (Lu, 2014). This parameter is symbolically denoted as  $ZT$  and defined in the equation below (Rowe, 2012).

$$ZT = \frac{S^2 \sigma T}{\kappa} \quad (2.1)$$

where

$S$  = Seebeck coefficient,  $VK^{-1}$

$\sigma$  = electrical conductivity,  $S \cdot cm^{-1}$

$\kappa$  = thermal conductivity,  $W \cdot m^{-1} \cdot K^{-1}$  (some texts also denote thermal conductivity as  $\lambda$ )

$T$  = absolute temperature when the above properties are measured, K

$S^2 \sigma$  = electron power factor,  $W \cdot m^{-1} \cdot K^{-2}$

It is more desirable to have larger  $ZT$  value which directly proportional to Seebeck coefficient, electrical conductivity and absolute temperature; inversely proportional to thermal conductivity. Since the invention of thermoelectric devices, intensive research and resources were invested to find thermoelectric materials that possess high  $ZT$  value. It was observed that metal or metal alloys (contain most free carriers, high thermal conductivity, albeit high electrical conductivity) and insulator (contain least free carriers, low thermal conductivity but also low electrical conductivity) often have low  $ZT$  value (much lesser than 1). In contrast, semiconductors have balanced behaviours between insulator and metal which show greater  $ZT$  values amongst others (Lu, 2014). This advantage is ascribed to the favourable physical property of semiconductors which have carrier (free electrons) density in between the range of  $10^{19}$  and  $10^{21} \text{ cm}^{-3}$  (Lu, 2014; Ma et al., 2021).

Figure 2.2 depicts the relationship between  $ZT$  value and carrier concentration (Ma et al., 2021).

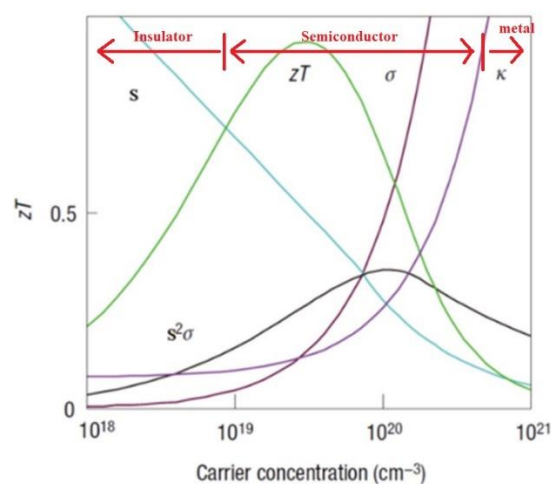


Figure 2.2: The Relationship between Carrier Concentration of a Thermoelectric Material and the  $ZT$  Value Together with Other Thermoelectric Parameters. Reprinted from Materials Science in Semiconductor Processing, 121/105303, Ma et al., Review of Experimental Approaches for Improving  $ZT$  of Thermoelectric Materials, Copyright 2021, with Permission from Elsevier.

Traditionally, emphasis was placed on searching novel materials or composites that could produce elevated  $ZT$  value. The identified and widely reported thermoelectric materials include  $\text{Bi}_2\text{Te}_3$  (bismuth telluride),  $\text{PbTe}$  (lead(II) telluride),  $\text{SrTiO}_3$  (STO: strontium titanate),  $\text{SnO}_2$  (tin dioxide) (Ferreira et al., 2015), and many others, where TEGs made of  $\text{Bi}_2\text{Te}_3$  ( $ZT$  value up to 0.97) are even commercialized nowadays (Wu et al., 2022). In conjunction with doping process which could considerably boost their thermoelectric performance (Saber and Sajjadi, 2022), significant improvements in synthesizing thermoelectric materials with higher  $ZT$  value are achieved by reducing its thermal conductivity,  $\kappa$ . Lu (2014) further elaborated that thermal conductivity of a thermoelectric material comprises a few decisive factors. The factor that has the most influential impact toward its thermal conductivity is the geometry arrangement of atoms. A large portion of overall  $\kappa$  (thermal conductivity) that is built up by this factor is known as lattice contribution (denoted as  $\kappa_L$ , some texts also refer it as lattice thermal conductivity). Numerous endeavours were therefore evolved to reduce this

lattice thermal conductivity which shrinks the performance of a thermoelectric device. Notably, phonon-grain boundary scattering is an effectual and proven mechanism which essentially obstructs heat transmission carried out by phonon (Liu, Ren and Chen, 2013). Practically, this method utilises nanotechnology to create a large density of grain interfaces or boundaries to restrict phonon transition, and yet allow carrier (electron or hole) to freely move within the thermoelectric material. This technique is known as nanostructuring and its outcomes such as nanoparticles, nanotubes, nanocoating, nanofilms, and so on are collectively addressed as nanostructured materials (Rafique et al., 2020). If the nanostructured materials retain thermoelectric properties, they are referred as nanostructured thermoelectric materials (Liu, Ren and Chen, 2013). Unlike usual thermoelectric materials, nanostructured thermoelectric materials concurrently show good electron power factor ( $S^2\sigma$ ) and low thermal conductivity ( $\kappa$ ) (Liu, Ren and Chen, 2013).

## **2.7 Nanostructured Thermoelectric Materials**

Before diving into the understanding of nanostructured thermoelectric materials, it is helpful to first comprehend the meaning of nanomaterials. There exist several definitions of nanomaterials according to different professional bodies (Kreyling, Semmler-Behnke and Chaudhry, 2010). For instance, International Organization for Standardization (ISO) postulated nanomaterials by their external dimension, internal structure, and external structure all in nanoscale (Boverhof et al., 2015). Specifically, nanomaterials appear in particulate form range from 1 nm to 100 nm (Carlander and Skentelbery, 2021) had raised concern in the scientific community. Kreyling, Semmler-Behnke and Chaudhry (2010), a joint effort between researchers from Germany and United Kingdom, commented that the range specified by ISO is vague neither providing a clear boundary for legislative bodies nor a practical evaluation criterion to distinguish nanomaterials from other materials. It is because nanomaterials might appear in aggregate or agglomerated assembly due to its inter-particles force. Moreover, nanomaterials possess some unique properties which are absent from traditional materials primarily because of their large surface area and quantum effects (Wu et al., 2020). As a

result, Kreyling and team suggested a new parameter, volume specific surface area (VSSA), to effectively determine whether a substance is a nanomaterial. That is, if the substance has  $VSSA \geq 60 \text{ m}^2/\text{cm}^3$ , it is a nanomaterial. This parameter compensates some limitations of previously defined meaning of nanomaterial. It basically means for a material of volume  $1 \text{ cm} \times 1 \text{ cm} \times 1 \text{ cm}$ , if its main particles have total surface area of  $60 \text{ m}^2$  or more, it is a nanomaterial.

Next, given a clearer image of nanomaterial, nanostructured materials explicitly refer to materials that have fundamental structural unit appeared in nanoscale which may also come in different dimensions. For instance, 0-dimension nanostructured materials refer to nanoparticles; 1-dimension nanostructured materials include nanofiber, nanowire, and nanotube; 2-dimension nanostructured materials point to thin layer(s), superlattices, or multilayers system (Rafique et al., 2020); and lastly 3-dimensional bulk nanocomposites. Nanocomposites are building blocks of nowadays nanostructured thermoelectric materials. There exist many fabricating methods of producing them and one of the simplest methods is by grinding an ingot into fine nanoparticles using high power ball-milling approach. The fine nanoparticles are then being transferred to hot-pressing station to eventually become a nanocomposite under appropriate pressure and temperature. In addition to hot-pressing method, spark plasma sintering method is also another preferred method to fabricate nanostructured thermoelectric materials. Both of these methods ensure the density of the thermoelectric materials is tally with the theoretical value. It was reported that a high-energy ball-milled and hot-pressing treated TE material  $\text{Bi}_x\text{Sb}_{2-x}\text{Te}_3$  could reach a record breaking  $ZT$  value of 1.4. Previously, maximum  $ZT$  value of thermoelectric materials fabricated via conventional methods is thought to be limited at 1.0 (Liu, Ren and Chen, 2013).

## **2.8 Transparent Thermoelectric Generator**

In fact, most of the traditional thermoelectric materials are opaque which limits their functionalities in advanced applications. These advanced applications include imperceptible prosthetics, imperceptible soft robotics (ISR), self-powered wearables, untethered robotic systems (Won et al., 2021),

internet-of-things (IoT) (Sun et al., 2021), power generating windows (Lee et al., 2021) and many others. Imperceptible robotics is often transparent (some are even flexible) or able to alter its colour / appearance according to surrounding environment, making them less perceptible to human vision. This characteristic is exceptionally important when it comes to biomedical services (Kaltenbrunner et al., 2013), undercover operations, and military missions which the robotics should not be seen by others (Morin et al., 2012). If they can obtain sufficient electrical power from high-performance transparent TEG, embedded battery pack, external power source and wires can therefore be spared, achieving totally self-powered mechanism. Apart from that, for more common daily usage, transparent TEG that can possibly replace traditional windows and at the same time generating electricity, is very prompting and ideal for sustainable development.

## **2.9 Transparency of a Material**

In general, when light particles (photons) strike on an object, a portion of its energy is absorbed by the object while the rest is being reflected. In subatomic perspective, the photon energy absorbed excites the valence electron(s) to jump from a lower-energy electron orbit to a higher-energy electron orbit. The amount of energy required to complete this electron excitation is known as optical bandgap. Different materials possess different optical bandgaps, some are higher while some are lower. Besides, visible light spectrum has wavelength ranged from 400 nm (violet) to 800 nm (red) which equivalent to energy (electronvolt) of around 3.26 eV to 1.65 eV (Prangnell, n.d.). For some materials which optical bandgap is greater than the maximum energy visible light can provide, the photon will not be absorbed by its valence electron(s) but instead penetrated through the object body. This essentially differentiates materials into optically transparent or opaque materials (Miodownik, M, 2014).

With basic knowledge of material transparency in mind, it is helpful to understand why some TEGs appear transparent. Transparent TEGs have been a focus. Multifold novel materials and structural morphologies are emerging to enhance its thermoelectric and mechanical properties. Some broadly discussed materials among scientific literature include polymer, organic / inorganic thin films, metal / alloy nanowires, and other

nanocomposites. Furthermore, some successful fabricated examples of transparent TEGs from other researchers are reported in the following subsection.

### **2.10 Examples from Other Researchers**

A Japanese team had synthesized a transparent and flexible TEG using Ga-Sn-O (GTO) thin film. The GTO thin film (thickness around 200 nm to 260 nm) was built on top of a glass substrate utilising radio frequency (RF) magnetron sputtering method. On top of the GTO thin film, a layer of 100 nm thick titanium (Ti) was deposited followed by another 20 nm thick layer of gold (Au). The module was then annealed under different combinations of four temperatures (100 °C, 200 °C, 300 °C, and 400 °C) and three Ar:O<sub>2</sub> ratios (20:0, 20:05, and 20:1). Their experiment results shown the highest power factor of 6  $\mu\text{Wm}^{-1}\text{K}^{-2}$  occurred when annealing temperature and Ar:O<sub>2</sub> ratio were fixed at 200 °C and 20:0, respectively (Yamamoto et al., 2021). However, the team neither further elaborated the reasons behind of choosing GTO, Ti, and Au as thermoelectric materials nor its important parameters such as thermoelectric figure of merit and output voltage. Nevertheless, their work introduced the possibility of selecting GTO as a suitable thermoelectric material candidate.

In another attempt performed by Kimura et al. (2022), a number of GTO thin-film TEGs were constructed using three different methods (radio frequency magnetron sputtering, room-temperature sputtering and mist chemical vapor deposition). Regardless of how the thermoelectric generators were made, they all had a layer of titanium (Ti) and gold (Au) on top to serve as terminals (temperature gradient was applied across these terminals and the output voltage difference across these terminals were measured). The structure is shown in Figure 2.3 next page. Among all three methods, the GTO TEG produced using mist chemical vapor deposition method yielded the highest output power factor of 59.8  $\mu\text{Wm}^{-1}\text{K}^{-2}$  where the composition ratio of Sn acetylacetonate and Ga acetylacetonate was set to 1 : 3.5. Although the latter journal provided more in-depth experimental procedures and analysis, it still did not clarify if GTO acted as a P-type or N-type material. Nonetheless, both

journals are good references to expand the knowledge and availability of transparent inorganic thermoelectric materials.

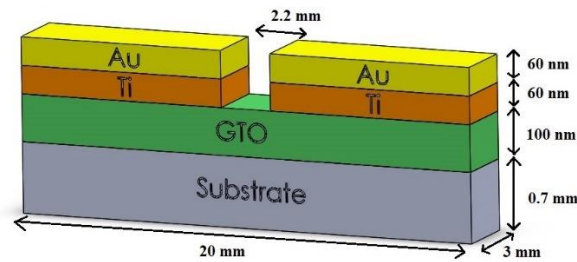


Figure 2.3: Structure of GTO Thermoelectric Generator Proposed by Yamamoto et al. (2021) and Kimura et al. (2022).

Usage of conductive polymers especially poly(3,4-ethylenedioxythiophene) (PEDOT) as a thermoelectric material is widely investigated and demonstrated by researchers globally. In a work showcased by Noh et al. (2014), the South Korean researchers successfully synthesized a transparent AgNWs (silver nanowires) – hcPEDOT (highly conductive PEDOT) electrode with an intention to replace the high-cost, industrialized ITO (indium tin oxide, a type of transparent conductive oxides) and to introduce an organic solar cell (OSC) which could be mass-produced. In other words, the process to manufacture indium tin oxide films is costly due to indium being scarce and expensive. Although the electrode was fabricated with a relatively low price and easy method, it has a surprising result in making the solar cell to reach a cell-efficiency of 2.16% when the solar cell was exposed to a solar simulation condition of 100 mW per centimetre square and standard sun spectrum (air mass 1.5 global). The group found that AgNWs which had many desired characteristics such as low electrical resistance, high transparency, and good elasticity could be used to make an electrode very similar to the electrical performance of an ITO electrode.

However, AgNWs needed a robust substrate in order to be meaningful for any practical applications. As a result, the team took the advantages of highly conductive (up to 700 S/cm) PEDOT (treated by DMSO) which is resistive and flexible as a supporting agent of the AgNWs. Moreover, this AgNWs/hcPEDOT composite film could be incredibly-easily obtained through spray-coating method. The only preparation step was to mix AgNWs with

hcPEDOT. Before the prototype was tested, another layer of PEDOT:PSS was sprayed on top of the AgNWs/hcPEDOT composite film to serve as a protective shield / buffer layer and to boost performance. The thickness of this composite film varies according to the spraying duration, the longer the spraying duration, the thicker the composite film but also the lower the optical transmittance. Their results shown that spraying period of 30s produced an AgNW/hcPEDOT of greatest PCE (power conversion efficiency) where the airbrush nozzle was 25 cm away from the substrate. Nevertheless, the AgNWs/hcPEDOT composite film in this work was only used as an anode, in fact there existed another cathode made from Ca/Al alloy to complete the solar cell circuit. More importantly, the backbone principle of generating electricity reported in their journal is through photovoltaic principle but not thermoelectric principle. Therefore, this journal can only serve as a study material. In fact, this research project initially had a high expectation to make use of AgNWs as one of the transparent electrode. However, there exists only few journals reporting on TEG made out of AgNWs.

Besides, the thermoelectric properties derived from the combination of AgNWs and poly(3,4-ethylenedioxythiophene) polystyrene sulfonate (PEDOT:PSS) were also studied in details by Yoshida and Toshima (2016). They prepared two AgNWs of different length, one at 3  $\mu\text{m}$  while another at 27  $\mu\text{m}$  and observed how these two different lengths of AgNWs would alter the thermoelectric properties of the PEDOT:PSS. They concluded that the electrical conductivity ( $\sigma$ ) of the AgNW/PEDOT:PSS film was proportional to the concentration of the AgNWs colloidal dispersion and AgNWs of longer length yielded higher electrical conductivity ( $\sigma$ ) possibly due to formation of more percolated nanostructures among them.

They managed to achieve a peak electrical conductivity ( $\sigma$ ) of 10000  $\text{Scm}^{-1}$  (reportedly 10 times greater than plain PEDOT:PSS) in their experiment. Interestingly, the high concentration of the AgNWs had significant contrary effect on the Seebeck coefficient (S) of the AgNW/PEDOT:PSS film. The team ascribed this phenomenon to increased number of free carriers. Decrease in Seebeck coefficient is not desired as it could exponentially downgrade the thermoelectric performance, provided that electron power factor, P is equal to  $S^2\sigma$ . The team claimed that integration of silver nanowires and PEDOT:PSS

did not seem to be helpful in fabricating a high-performance thermoelectric material. Thus, their work reserves a doubt that synthesizing a thermoelectric generator using AgNWs/PEDOT:PSS might not be a wise direction.

Lastly, in the work carried by Wang, et al (2020) from Agency for Science, Technology and Research (A\*STAR), Singapore, they fabricated a transparent yet flexible TEG (f-TEG) using PEDOT:PSS (post-processed by trifluoromethanesulfonic, TFMS acid to boost Seebeck coefficient and electrical conductivity) as p-type pairing leg and ITO as n-type pairing leg. Instead of connecting both legs using conventional metal electrodes, such as silver or copper wire, they innovatively overlapped the PEDOT:PSS and ITO to achieve the p-n junction functionality. The PEDOT:PSS thin film of thickness 65 nm was deposited on a transparent substrate (glass) through spin-coating method and the ITO thin films were obtained by using radio frequency (RF) magnetron sputtering method where the processing temperature was maintained around 60 °C. The group claimed that their prototype exhibited exceptionally excellent properties such as transparency of more than 81% (between visible wavelength 400 – 800 nm) and a record-breaking output power density of 22.2 Wm<sup>-2</sup>. These well-founded qualities reportedly ascribed their TEG module to be of the optimal performance as compared to other previously fabricated hybrid/organic f-TEGs. The fabrication process of this thermoelectric generator was relatively feasible within a laboratorial setting and its persuasive power generating capability have served as a promising reference in this paper.

Table 2.1 tabulates some thermoelectric materials investigated by other researchers and also some of their important parameters.

Table 2.1: TEG Modules Reported by Other Researchers and Their Respective Parameters.

p - type	Peak ZT	n-type	Peak ZT	transmittance*	Power density	Power factor	Reference
$\text{Bi}_{0.4}\text{Sb}_{1.6}\text{Te}_3$	-	$\text{Bi}_{1.75}\text{Te}_{3.25}$ (bismuth telluride)	-	opaque	33.33 $\text{Wm}^{-2}$ ( $\Delta T=20\text{K}$ )	-	(Inayat, Rader and Hussain, 2014)
PEDOT:PSS	0.3 (450K)	ITO	0.29 (450K)	> 81% (400 – 800 nm)	22.2 $\text{Wm}^{-2}$ ( $\Delta T=80\text{K}$ )	-	(Wang et al., 2020)
-	-	$\text{TiO}_2:\text{Nb}$ (Niobium-doped titanium dioxide)	0.014	73% (400 – 700 nm)	-	60 $\mu\text{Wm}^{-1}\text{K}^{-2}$	(Ribeiro et al., 2021)
CuI films	0.21 (300K)	-	-	80% – 95% (300 – 1100 nm)	-	17 $\mu\text{Wm}^{-1}\text{K}^{-2}$	(Vora-ud et al., 2022)
CuI films	0.29	GZO film (gallium doped zinc oxide)	0.07	70% – 80% (400 – 800 nm)	10.83 nW ( $\Delta T=20\text{K}$ )	-	(Coroa et al., 2019)
-	-	AZO film (aluminium zinc oxide film)	0.1 (at room temperature)	80% (400 – 800 nm)	-	400 $\mu\text{Wm}^{-1}\text{K}^{-2}$	(Loureiro et al., 2014)
PEDOT:PSS	-	constantan	-	opaque (flexible)	-	10.14 $\mu\text{Wm}^{-1}\text{K}^{-2}$	(Zeng et al., 2022)
$\text{FeCl}_3$ -MWCNT ( $\text{FeCl}_3$ -treated-MWCNT film)	0.016 (300K)	PEI-CNT (PEI-treated-CNT film)	0.0073 (300K)	opaque (flexible)	1.409 $\text{Wm}^{-2}$ ( $\Delta T=38.9\text{K}$ )	-	(Wu et al., 2021)

\* visible wavelength falls between 400 nm (violet) and 800 nm (red) (Bastiaansen et al., 1993).

## 2.11 Summary

In a nutshell, after comparing all research works performed by other researchers and scholars, making a transparent thermoelectric generator (t-TEG) was totally feasible under UTAR Sungai Long Campus laboratory setting. The particular t-TEG module demonstrated by Wang et al. (2020) which shown a record-breaking output power density of  $22.2 \text{ Wm}^{-2}$  ( $\Delta T=80\text{K}$ ) is an auspicious reference to realize the objectives. Although UTAR laboratory inventory did not equip with TFMS which was used by Wang et al. (2020) to increase the Seebeck coefficient of PEDOT:PSS, pure PEDOT:PSS with ITO combination was instead utilized to realize a t-TEG. Its output parameters (output voltage, output current and output power) are benchmarked in this project, and discussed in the next chapter.

## CHAPTER 3

### METHODOLOGY AND WORK PLAN

#### 3.1 Introduction

This research project applied a systematic approach to firstly explore the basic working principle of a t-TEG and thereby verified its feasibility and characterized its output parameters. It involved both qualitative and quantitative methodologies. The former referred to literature review and case studies where multiple researchers reported different combinations of materials to make t-TEG. From there, t-TEG of reportedly highest output performance was chosen and fabricated in this research project. On the other hand, the quantitative methodology kicked in primarily in May 2022 trimester where laboratory experiments were being carried out to fabricate the chosen t-TEG and characterized its output parameters. The experimental procedures were documented in detail in the following subsections to ensure the result's repeatability. Last but not least, the experimental results were analysed and discussed to acquire more insight of this emerging t-TEG and its relatively new applications.

##### 3.1.1 Introduction to Spin Coating Method

Spin coating method is a technique widely employed in laboratory level to make thin films or membranes due to its simplicity and rapid outcomes (Chen et al., 2018). Its primary mechanical components involve a flat circular disk (known as wafer) and a motor. The bottom of the wafer is locked together with the shaft of the motor and both are aligned concentrically (Smith, Peters and Inomata, 2013). Some spin coaters have added functionalities such as enabling the temperature control of the spinning environment (Nguyen, 2012). Moreover, the rotational speed of the motor is adjustable and therefore the wafer can rotate at different pre-set speeds. Here, a solution / liquid is dropped onto a substance (e.g., glass or silicon) and placed on top of the wafer. As soon as the wafer starts spinning, the centrifugal force and surface tension induce

the solution / liquid to spread out evenly on the substrate, results in a uniform and thinner layer covering the substrate (Makhlouf, 2011). The thickness of the resulting thin film can range from nanometers to micrometers (Paras and Kumar, 2021). The factors influencing its resultant thickness include the spinning speed, viscosity of the solution / liquid, concentration of the solution, vapour pressure, and temperature (Buonomenna, 2016). Furthermore, this whole process can be repeated by adding more solution / liquid to subsequently increase the thickness of the thin film (Fourati et al., 2016). Figure 3.1 illustrates the schematic diagram of a spin coater.

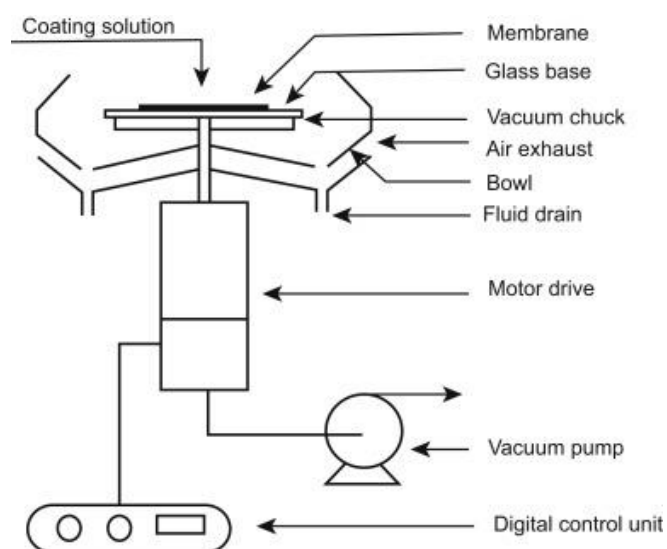


Figure 3.1: Schematic Diagram of a Spin Coater. Reprinted from *Current Trends and Future Developments on (Bio-) Membranes: Photocatalytic Membranes and Photocatalytic Membrane Reactors*, (Chen et al., 2018), *Materials and Design of Photocatalytic Membranes*, pg. 71-96, Copyright 2018, with Permission from Elsevier.

### 3.1.2 Introduction to Corona Treatment

Corona treatment was a common industrial practice to enhance surface energy of a substrate (plastic packaging, foil, LDPE, polymers, or glass) before printing. The devices to perform corona treatment include a transformer, a generator and electrodes. Corona discharge could be seen between the electrode and the substrate, which was also described as plasma. Although the excited electrons carried a temperature of about 100 thousand K, it hardly caused any damage to the substrate due to electron's trivial heat capacity (Izdebska, 2016). Corona treated substrates had greater liquid adherence which in layman terms, the ink / liquid could adhere to the substrate stronger, creating a bond between two different materials (Vetaphone, 2020). Therefore, all glass substrates in this experiment underwent corona treatment to create a stronger bond between PEDOT:PSS and the glass substrate itself. PEDOT:PSS would poorly stick to the glass substrate if corona treatment was not performed beforehand. Figure 3.2 shows the handheld corona treater purchased from Electro-Technic Products INC., USA. It consists of four main components, namely generator handle, electrode, power control source (transformer), and plug.

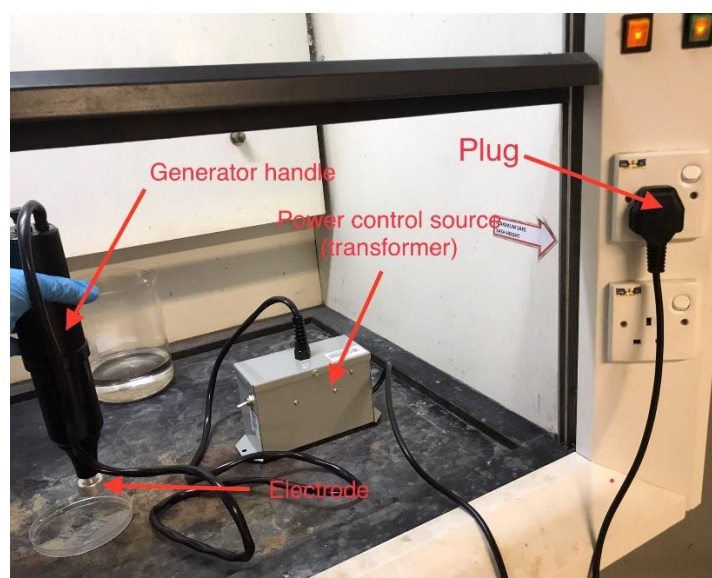


Figure 3.2: Four Main Components of the Handheld Corona Treater.

### 3.2 Locations, Equipment and Materials

Each department could provide different services and equipment that were necessary to fabricate the t-TEG. Most equipment / items were stored in various places and sometimes it could be very difficult to locate them. Therefore, Table 3.1 records all locations where the necessary items / equipment / services could be found.

Table 3.1: Locations and Their Services Provided.

Locations	Services provided
KB613 Robotics & Automation Laboratory	<ol style="list-style-type: none"> <li>1. Keithley 6514 System Electrometer</li> <li>2. Ossila Four-Point Probe</li> <li>3. Jumper wire</li> <li>4. Soldering kit</li> </ol>
KB614 Biomedical Engineering Laboratory	<ol style="list-style-type: none"> <li>1. Locker rental</li> <li>2. Micropipette rental</li> <li>3. First aid kit</li> </ol>
KB615 Molecular & Tissue Engineering Laboratory	<ol style="list-style-type: none"> <li>1. Main working desk with 12 power sockets</li> <li>2. Distilled water</li> <li>3. Hand gloves</li> <li>4. WYPALL<sup>®</sup> jumbo roll wiper</li> <li>5. Fume hood</li> <li>6. Kimtech<sup>™</sup> Science Kimwipes delicate task wipers</li> <li>7. Refrigerator</li> </ol>
KB724 Materials & Manufacturing Engineering Laboratory	<ol style="list-style-type: none"> <li>1. Hot plate rental</li> <li>2. WYPALL<sup>®</sup> jumbo roll wiper</li> <li>3. Aluminium foil</li> </ol>
KB725 Heat treatment & Furnace Laboratory	<ol style="list-style-type: none"> <li>1. Diamond glass cutter</li> <li>2. Spin coater</li> <li>3. Fume hood</li> <li>4. Laboratory corona treater</li> <li>5. Hand gloves</li> </ol>
KB728 Chemical Engineering Laboratory	<ol style="list-style-type: none"> <li>1. Fume hood</li> <li>2. Disposal of glass waste, used hand gloves and micropipette tips</li> </ol>
KB730 Applied Mechanics Laboratory 2	<ol style="list-style-type: none"> <li>1. Main switch to turn on air compressor for spin coating</li> </ol>
KB Level 7 LKC FES Researcher Steel Cabinet No. 7-SCR15	<ol style="list-style-type: none"> <li>1. Kimtech<sup>™</sup> Science Kimwipes delicate task wipers</li> <li>2. Micropipette tips</li> </ol>

In addition, all equipment and materials used in this research project were listed in Table 3.2.

Table 3.2: Equipment and Materials.

Item Description	Item category*	Quantity estimation
CJMCU-3108 ultra-low voltage booster breakout board	W	1 unit
Coilcraft transformer LPR6235-752SML (1:100 ratio)	W	1 unit
Computer	E	1 unit
Conductive copper tape	C	2 cm
CORNELL DUBILIER Supercapacitor EDS104Z5R5C 0.1F, 5.5V, 85°C	W	1 unit
Diamond glass cutter	W	1 unit
Epoxy hardener B	C	10 ml
Epoxy resin A	C	10 ml
Hot air gun	E	1 unit
Hot plate	E	1 unit
Iso Propyl Alcohol C <sub>3</sub> H <sub>8</sub> O	CH	2 sprays
ITO glass	SP	1 slide
Jumper wire	C	15 cm
Keithley 6514 System Electrometer	E	1 unit
Keithley IVI-COM/IVI-C driver	S	1 unit
Kimtech™ Science Kimwipes delicate task wipers	C	2 sheets
Laboratory corona treater	W	1 unit
Micropipette (20 µL – 200 µL)	W	1 unit
Micropipette tip	C	1 unit
Microscope slides	C	1 slide

Ossila Four-Point Probe	E	1 unit
PEDOT:PSS solution	CH	200 $\mu$ L
Plastic petri dish	W	1 unit
Soldering iron kit	E	1 unit
Spin coater	E	1 unit

Item category*	
C	Consumable
CH	Chemical
E	Equipment
S	Software
SP	Sample or specimen
W	Labware, glassware, tool, and components

### 3.3 Cost

Table 3.3 tabulates all items purchased and their respective price for this project. This table did not include items / equipment / apparatus that were readily available under UTAR laboratory inventory or provided by supervisor or seniors. Some other items purchased but later found not suitable to be used in this project were also being omitted from the table.

Table 3.3: Items Purchase and Their Price.

Item Name	Quantity	Price
Peltier_Tec1-12706	1	RM 12.99
Peltier SP1848	1	RM 13.99
CJMCU-3108 LTC3108-1 ultra-low voltage boost converter	1	RM 28.72
Stylish spray bottle SPR04 500ML	1	RM 3.90
Thermal sticker, 3M double-sided adhesive heat dissipation	1	RM 4.00
Clear epoxy 4 mins 2×17 ml	1	RM 7.70
1:100 transformer LPR6235-752SML	1	RM 22.59
Supercapacitor EDS104Z5R5C	1	RM 15.62
Selleys epoxy fix	1	RM 13.00
	Total:	RM 122.51

### **3.4 Transparent Thermoelectric Generator Fabrication**

This subsection attempts to demonstrate the fabrication of the t-TEG module that was made under UTAR Sungai Long Campus laboratory setting. It was planned out with result reproducibility and reliability in mind, together with a strong coherence to laboratory safety rules and regulations, fundamental working principles, and guidance to various tools and equipment. Moreover, it had undergone multiple amendments and improvements thorough the project execution and only the best method to make a t-TEG module was being reported here. By following this methodology, a t-TEG module which gave the optimal output voltage, output current, water and dust resistance, surface finishing, aesthetics, and durability could be reproduced. In this section, the step-by-step experimental procedures are reported and described in detail.

### 3.4.1 Procedure to Make Transparent Thermoelectric Generator

1. A small piece of glass (15 mm × 20 mm) was cut out from a microscope slide (25.4 mm × 76.2 mm) using diamond glass cutter. The shallow score created by the diamond glass cutter allowed the glass to break along the score when subjected to a small bending torque.
2. Iso propyl alcohol (C<sub>3</sub>H<sub>8</sub>O) was then sprayed on both sides of the small glass and wiped dry with Kimtech™ Science Kimwipes delicate task wipers.
3. The cleaned glass was then placed on a plastic petri dish and subjected to corona treatment using the handheld corona treater inside a fume hood. The generator handle was held upright, and its electrode was about 1 cm above the cleaned glass (as shown in Figure 3.3). The cleaned glass underwent at least 30 seconds corona treatment and eventually served as the substrate for PEDOT:PSS.

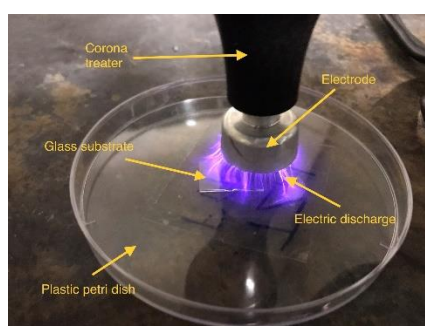


Figure 3.3: Corona Treatment on Glass Substrate.

4. Six pieces of corona treated glass substrates were fabricated by repeating step 1 to step 3.
5. The glass substrate was then transferred to the SCS 6800 spin coater and sat on the centre of the rotating plate which created suction to hold the glass substrate in place. Its corona-treated surface was facing upward.
6. 70 μL PEDOT:PSS solution was dropped onto the glass substrate using a micropipette (as shown in Figure 3.4).



Figure 3.4: 70  $\mu\text{L}$  PEDOT:PSS Solution on Glass Substrate.

7. The spin coating process was initiated with parameters adjusted as follow:
  - Ramp (s) = 0
  - Dwell (s) = 30 seconds
  - RPM = 2000 rpm
8. After the spin coating process was completed, the glass was removed from the rotating plate and placed on a preheated hot plate (100  $^{\circ}\text{C}$ ) for 1 minute.
9. There were five different PEDOT:PSS coated glasses being prepared according to Table 3.4. Each additional layer of PEDOT:PSS repeated step 6 to step 8.

Table 3.4: 5 Samples with Their Respective Number of PEDOT:PSS Layers.

Samples	Number of PEDOT:PSS layer(s)
First sample	1
Second sample	2
Third sample	3
Fourth sample	4
Fifth sample	5

10. The sixth and also the last PEDOT:PSS thin film sample was made without going through spin coating process. Instead, 100  $\mu\text{L}$  of PEDOT:PSS solution was evenly spread on a corona treated glass substrate and directly put on the 100  $^{\circ}\text{C}$  hot plate for 1 minute and let dry.

11. The PEDOT:PSS coated glass was then removed from the hot plate and connected to a ITO coated glass side-by-side with conductive copper tape. A TEG module consisted of p-type material (PEDOT:PSS) and n-type material (ITO) was now obtained.
12. Two 5 cm jumper wires were attached to the bottom corners of the TEG module with conductive copper tape adhering the wire to the glass.
13. 10 ml of epoxy resin A and 10 ml of epoxy hardener B were well mixed before the mixture was applied to the TEG module. Figure 3.5 shows the final prototype.

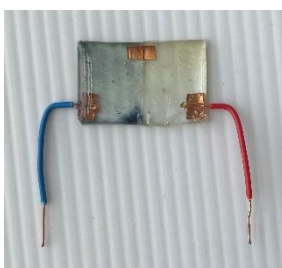


Figure 3.5: Final Prototype.

14. These six t-TEG modules were tested individually for its transparency, output voltage and output current when subjected to a temperature gradient from 0 °C up to 120 °C.
15. The TEG characterization was done by using Keithley 6514 System Electrometer where its positive probe (red colour) was connected to the PEDOT:PSS terminal and its negative probe (black colour) was connected to the ITO terminal.
16. The Keithley IVI-COM/IVI-C driver was downloaded from <https://www.tek.com/en/support/software/driver/keithley-ivi-com-ivi-c-driver-models-2450-2460-2461-2470-version> and installed onto a computer.
17. After that, the “K6514 Electrometer Suits” application was opened from the download directory: Keithley Electrometer > Keithley Electrometer 6514 Installation Files > K6514 Electrometer Suits > K6514 Electrometer Suits
18. After the application was opened, the “File” icon on the top left corner was clicked followed by the “Open” button.

19. The “K6514 Application.prj” file was selected from the subfolder: Keithley Electrometer > Keithley Electrometer 6514 Installation Files > K6514 Application.prj. The following menu appeared, and measurement was initiated by selecting the desired parameters (as shown in Figure 3.6).



Figure 3.6: K6514 Application Homepage.

20. Nine TEGs with non-spin-coated PEDOT:PSS were then fabricated by directly depositing 100  $\mu\text{L}$  PEDOT:PSS solution on a glass substrate and placed on a 40  $^{\circ}\text{C}$  hotplate to let dry.
21. TEGs with non-spin-coated PEDOT:PSS were connected in series and subjected to a temperature gradient from 0  $^{\circ}\text{C}$  up to 150  $^{\circ}\text{C}$ , and its output voltage and output current were measured.
22. Five of these TEGs with non-spin-coated PEDOT:PSS were connected in parallel and subjected to a temperature gradient from 0  $^{\circ}\text{C}$  up to 150  $^{\circ}\text{C}$ , and its output voltage and output current were measured.

### 3.4.2 Precaution

1. Hand gloves and laboratory coat were always worn especially handling chemicals and cutting glasses.
2. Pressing the diamond glass cutter against the microscope slide too hard could break the glass unexpectedly (as shown in Figure 3.7). Only adequate but not excessive force was applied when cutting the microscope slide.

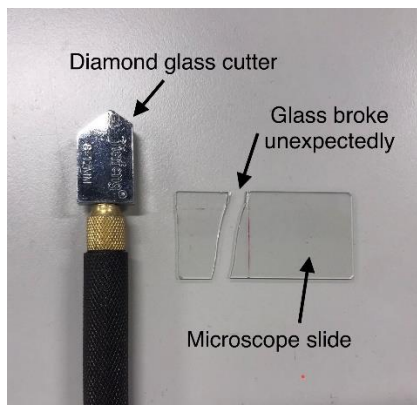


Figure 3.7: Avoid Excessive Force When Cutting Glass Substrate.

3. The corona treatment was carried out inside the fume hood and above a non-conductive plastic petri dish as people could be shocked by electricity if the electric discharge passed through other metallic bodies. The fume hood sash was pulled down below the maximum safe sash height (as shown in Figure 3.8).



Figure 3.8: Maximum Safe Sash Height.

4. In order to create an effective temperature gradient across the TEG module, the side without any jumper wire was immobilized on the edge of the hot plate and its another side was hanging in the air. Weights (metal tubes) were put on the hot side of the TEG module to hold the module in place (as shown in Figure 3.9).

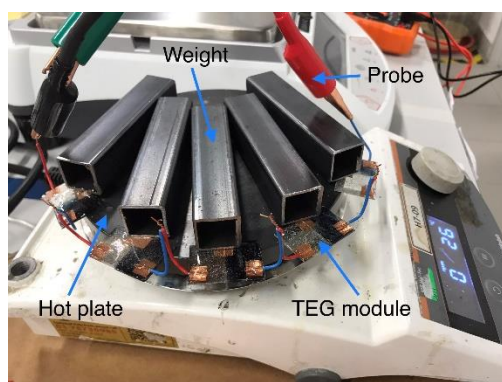


Figure 3.9: Example of an Experimental Set Up.

5. After each and every measurement done by the Keithley electrometer, the “Reset” button was clicked so that the next measurement could start from zero (as shown in Figure 3.10). Otherwise, the electrometer could yield false readings.



Figure 3.10: Reset Button.

6. The inner wall of the spin coater was often contaminated by the PEDOT:PSS solution after each spin coating process. Thus, it was cleaned with water and WYPALL® jumbo roll wiper every time so that it would leave no hassle for the next user.

### 3.5 CJMCU-3108 Ultra-low Voltage Booster Set Up

A boost convertor (CJMCU-3108 ultra-low voltage booster) was initially set up to intentionally boost up the output voltage from a t-TEG to a higher voltage that was sufficient to light up a LED. This boost convertor required a minimum input source of 20 mV and 3 mA to operate. Although this boost convertor was not later used to boost up voltage from a t-TEG mainly because the output current from TEG was lower than 3 mA, it still served as a good reference for further studies when the t-TEG has output current flow of more than 3 mA.

#### 3.5.1 Procedure to Set Up CJMCU-3108 Ultra-low Voltage Booster

1. The Coilcraft transformer LPR6235-752SML (1:100 ratio) was soldered onto the CJMCU-3108 ultra-low voltage booster breakout board using a hot air gun (as shown in Figure 3.11).

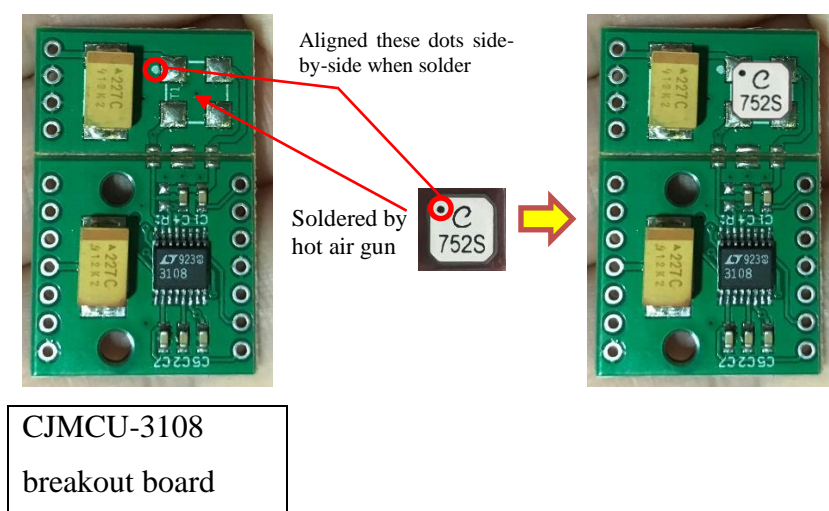


Figure 3.11: Soldering Transformer onto CJMCU-3108 Breakout Board.

2. The upper part and the lower part of the breakout board were connected by solder and pin headers were soldered to every pin of the breakout board (as shown in Figure 3.12).

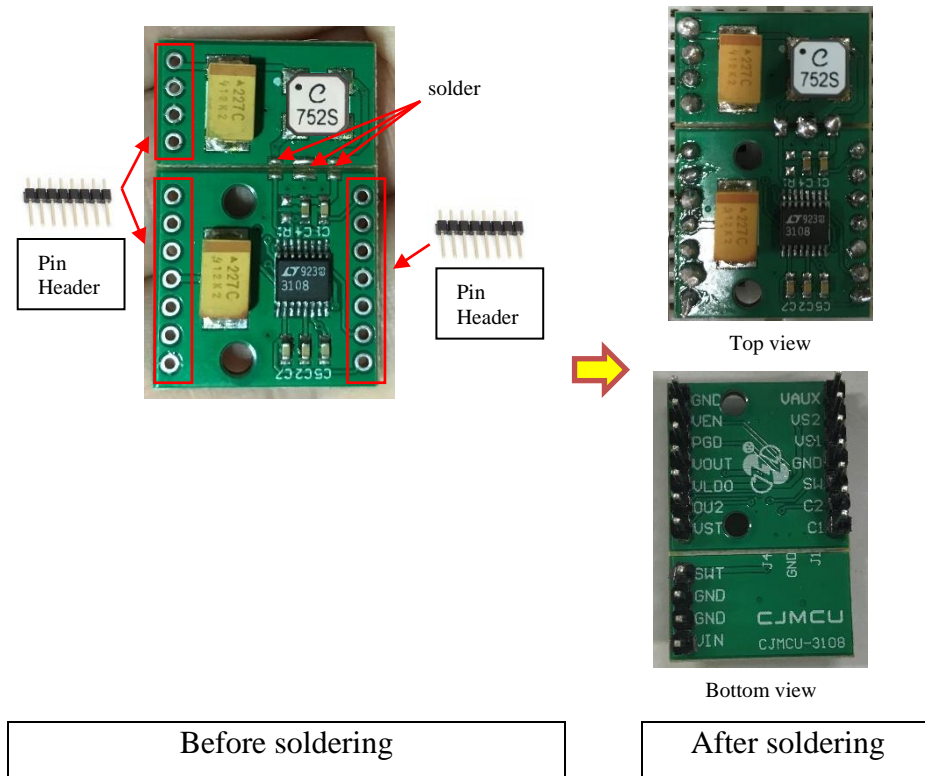


Figure 3.12: Soldering Pin Header onto CJMCU-3108 Breakout Board.

3. The CJMCU-3108 breakout board was then inserted onto a breadboard and some of its pins were connected via jumper wires. The wire connections were done by following a circuit diagram in a datasheet (LTC3108: Ultralow Voltage Step-Up Converter and Power Manager; accessible online through: <https://www.analog.com/media/en/technical-documentation/data-sheets/LTC3108.pdf>) provided by Analog Devices, Inc (as shown in Figure 3.13). This circuit diagram shows the wire connection to obtain a typical output power of 3.3 V which was boosted from an input of a Peltier cell (power source).

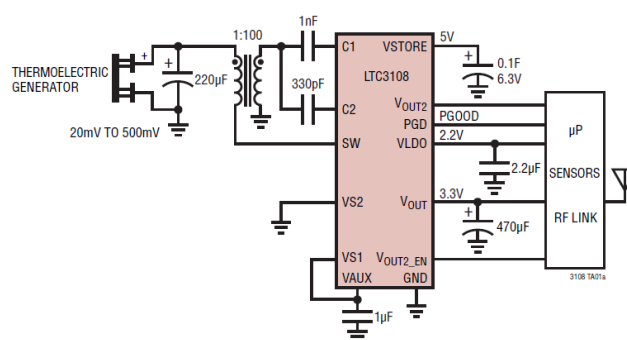


Figure 3.13: Circuit Diagram to Connect Pins on the CJMCU-3108 Breakout Board.

Most capacitors shown on Figure 3.13 were pre-soldered on the CJMCU-3108 breakout board. Therefore, the boost converter would start to function by simply connecting certain pins on the breakout board correctly using jumper wires. Table 3.5 in the next page summarized the connection of each pin and Figure 3.14 shows the schematic diagram of the entire connection.

Table 3.5: Transparency of Glass Substrate with Different PEDOT:PSS Layers

Pins on CJMCU-3108 breakout board	Connection
VIN	To the positive terminal (red wire) of Peltier cell.
GND	All GND pins connected together with the negative terminal (black wire) of Peltier cell.
VST	To the anode of the EDS104Z5R5C supercapacitor.
VOUT	To the anode of LED.
VAUX	To VS1 on the same board.
VS2	To ground together with the negative terminal (black wire) of Peltier cell.

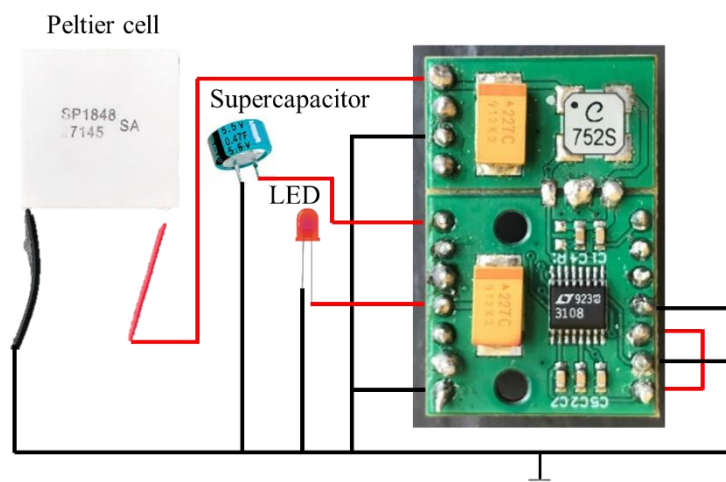


Figure 3.14: Actual Wire Connection of the CJMCU-3108 Breakout Board.

### **3.6 Summary**

This chapter documented all the steps and procedures to fabricate t-TEGs and to set up CJMCU-3108 boost convertor in a very detailed manner. A profoundly prepared work plan not only ease the experiment process but also ensure the objectives in this project could be achieved. In addition, the reported procedures could serve as a valuable guideline for juniors and upcoming scholars to conduct deeper investigation into the field of t-TEGs. There were 22 steps involved in fabricating a t-TEG and six precautions were being pointed out. On the other hand, there steps were elaborated in setting up a CJMCU-3108 boost convertor. The duration of conducting all experiments was 88 days, which commenced on 13 June 2022 and ended on 8 September 2022. The total cost involved in this project was RM 122.51 excluding items that were supplied by laboratory.

## CHAPTER 4

### RESULTS AND DISCUSSION

#### 4.1 Introduction

The experimental data was being collected as early as 1<sup>st</sup> of July 2022 and all necessary experiments were completed by 8<sup>th</sup> of September 2022. As mentioned in previous section, both output voltage and output current of TEGs were measured by Keithley 6514 System Electrometer. This electrometer could measure extremely small current (ranged from 100 aA until 20 mA) and also paired with more than two hundreds T $\Omega$  input impedance when measuring voltage (capable to measure voltage ranged from 10  $\mu$ V until 200 V) (Tektronix, 2022). The first part of the result discussed the output voltage and output current of t-TEGs which their PEDOT:PSS was spin-coated on a glass substrate. The second part of the result analysed the output voltage and output current of TEGs when the PEDOT:PSS was not spin-coated, i.e. direct deposition of 100  $\mu$ L of PEDOT:PSS solution on the glass substrate. The third part of this result shown the transparency of glass substrates with increasing layers of PEDOT:PSS thin films and the transparency of TEG modules before and after subjected to high temperature.

## 4.2 Output Voltage and Output Current of TEGs with PEDOT:PSS Spin-Coated

Table 4.1 tabulates the output voltages of five different TEG modules. Each TEG module had different amount of p-type material, PEDOT:PSS. The amount of PEDOT:PSS was controlled by the number of PEDOT:PSS thin layers which were spin-coated on respective glass substrate. The average output voltages of each TEG module when subjected to a set of temperature gradients,  $\Delta T$  ranged from 0°C up to 120°C were recorded. The highest output voltage of 0.5181 V was obtained when the TEG was subjected to a temperature gradient of 120 °C. The experimental setup is shown in Figure 4.1. Note that one side of the TEG is hanging in the air which served as cold side. Another side is stabilized by a weight on the hotplate which served as hot side.

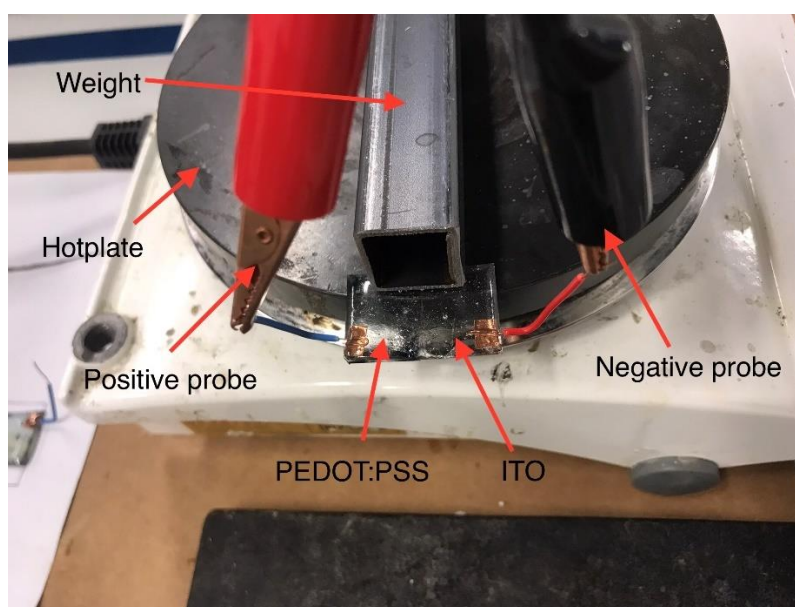


Figure 4.1: Experimental Setup to Characterize TEG (PEDOT:PSS Spin-coated).

Table 4.1: Output Voltage of a Single TEG with Different PEDOT:PSS Layer(s).

Temperature gradient, $\Delta T$ ( $^{\circ}\text{C}$ )	Output voltage (V)				
	1 layer PEDOT:PSS	2 layers PEDOT:PSS	3 layers PEDOT:PSS	4 layers PEDOT:PSS	5 layers PEDOT:PSS
0	-0.0102	0.0007	0.0206	0.0585	0.1411
10	-0.0156	0.0379	0.0928	0.0604	0.0414
20	-0.0197	0.0742	0.1503	0.0903	0.2007
30	-0.0228	0.1098	0.0760	0.1902	0.2357
40	-0.0173	0.1505	0.1295	0.2732	0.2427
50	-0.0132	0.1818	0.1363	0.1682	0.2454
60	0.0081	0.1025	0.1024	0.2103	0.3440
70	0.0082	0.2737	0.1570	0.1278	0.2816
80	0.0293	0.1818	0.1596	0.1504	0.3269
90	0.0345	0.3097	0.3881	0.1541	0.3330
100	0.2266	0.2039	0.2223	0.3396	0.4280
110	0.1742	0.1416	0.2772	0.3956	0.4710
120	0.2355	0.2972	0.4457	0.3821	0.5181

In addition, Figure 4.2 – 4.4 illustrate the output voltage of different t-TEGs across a set of temperature gradients. The output voltage posted a growing trend as the number of PEDOT:PSS layers increased from 1 layer to 5 layers. On the other hand, regardless how many PEDOT:PSS layers were coated, all TEGs output voltages were proportional to temperature gradient. For instance, when temperature gradient elevated from 10  $^{\circ}\text{C}$  to 120  $^{\circ}\text{C}$ , the output voltage of the TEG module with 5 layers of spin-coated PEDOT:PSS also rose from 0.0414 V to 0.5181 V.

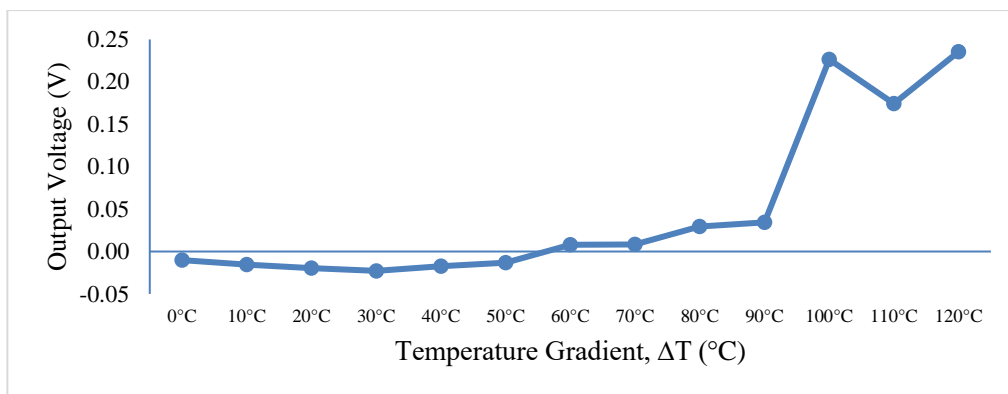


Figure 4.2: Output Voltage vs Temperature Gradient (1 Layer PEDOT:PSS).

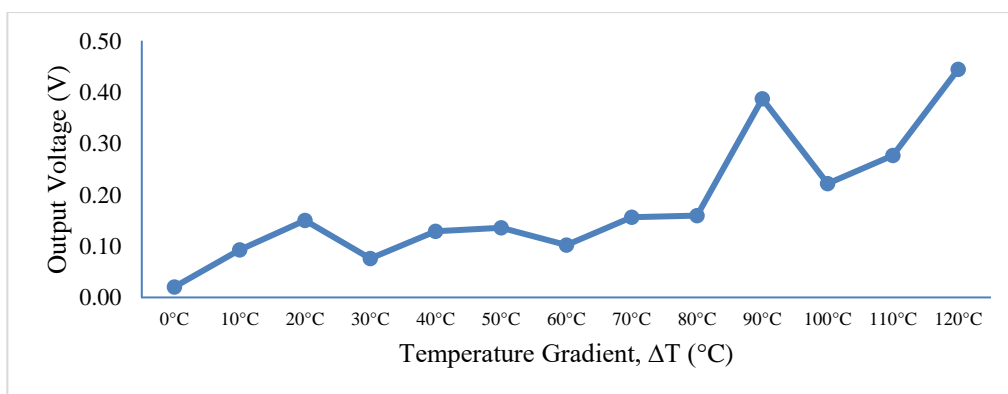


Figure 4.3: Output Voltage vs Temperature Gradient (3 Layers PEDOT:PSS).

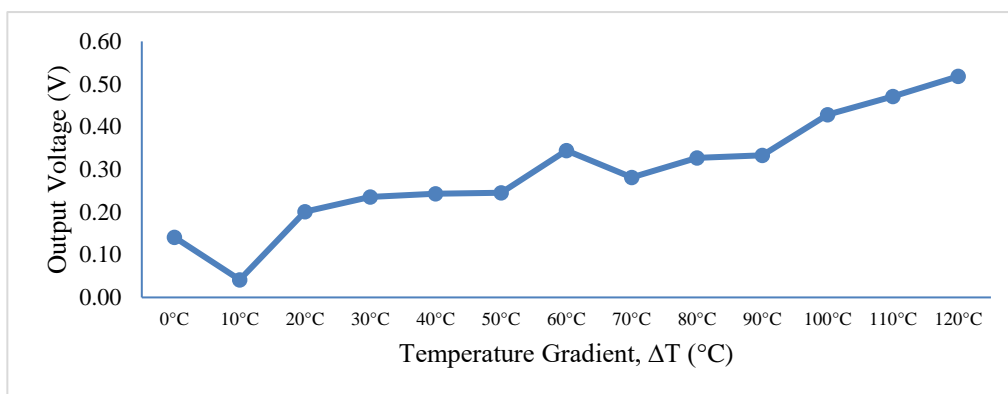


Figure 4.4: Output Voltage vs Temperature Gradient (5 Layers PEDOT:PSS).

Although the output voltages were within the expectation of 0.2 V to 0.5 V, the output currents of all fabricated TEGs module were astonishingly low. Referring to Table 4.2, the highest output current obtained from the TEG module with five PEDOT:PSS layers, stood only at 62.66 nA under a temperature gradient of 120 °C. Furthermore, the output currents show an increasing trend as the temperature gradient increases. This phenomenon is similar to that of the output voltage discussed by other researchers. It could be drawn to a facile conclusion that the higher the temperature gradient, the more power (output voltage  $\times$  output current) the TEGs could yield. Besides, Figure 4.5 – 4.7 show the significance of number of PEDOT:PSS layers on the overall output current. TEG modules with 1 to 4 PEDOT:PSS layers failed to pass the 10 nA output current benchmark, while TEG module with 5 PEDOT:PSS layers spiked from 6.11 nA to 50.88 nA when the temperature gradient increased to 80 °C and above.

Table 4.2: Output Current of a Single TEG of Different PEDOT:PSS layer(s).

Temperature gradient, $\Delta T$ (°C)	Output current (nA)				
	1 layer PEDOT:PSS	2 layers PEDOT:PSS	3 layers PEDOT:PSS	4 layers PEDOT:PSS	5 layers PEDOT:PSS
0	-0.1275	-0.0059	-0.0136	-0.8877	1.4370
10	-0.0040	0.0054	0.0118	-0.2128	1.0587
20	-0.0015	0.0139	0.0107	0.0556	2.1450
30	-0.0002	0.0118	0.0673	0.0551	2.7280
40	-0.0037	0.0104	0.0692	0.0470	3.1320
50	-0.0034	0.0186	0.0959	0.0817	4.3590
60	-0.0067	0.0723	0.1543	0.1137	4.2000
70	-0.0053	0.1155	0.1377	0.7581	6.1050
80	-0.0011	0.1797	0.1368	0.7133	50.8800
90	-0.0008	0.1339	0.0881	1.7735	53.4900
100	0.0851	0.6887	0.5743	2.6338	56.8500
110	0.1130	1.1799	0.9062	2.5410	59.5700
120	0.0978	0.9167	1.2138	5.8980	62.6600

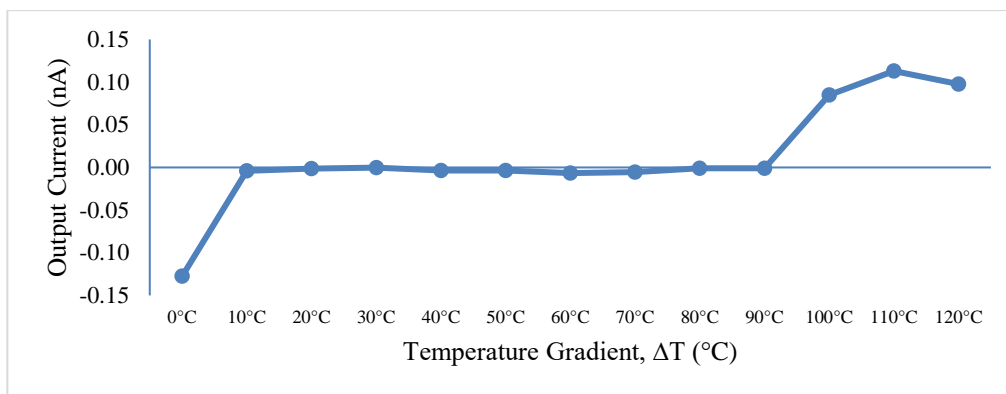


Figure 4.5: Output Current vs Temperature Gradient (1 Layer PEDOT:PSS).

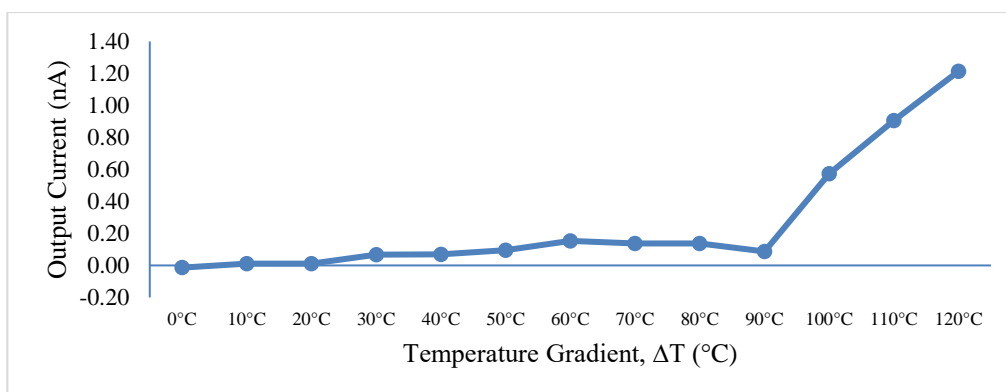


Figure 4.6: Output Current vs Temperature Gradient (3 Layers PEDOT:PSS).

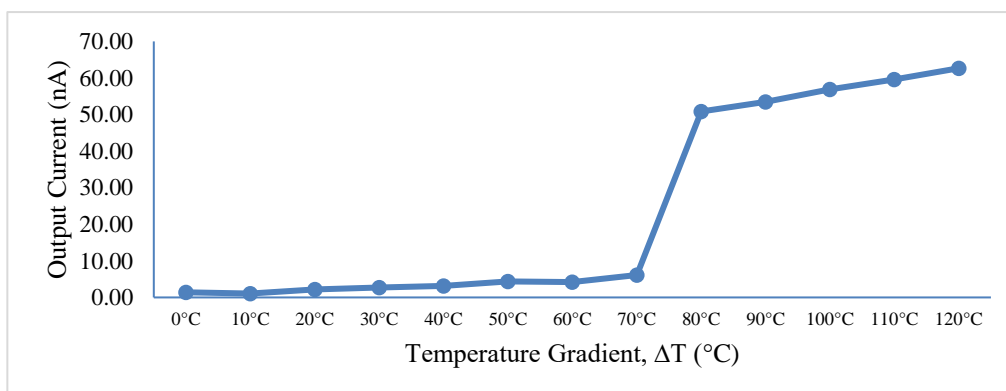


Figure 4.7: Output Current vs Temperature Gradient (5 Layers PEDOT:PSS).

### 4.3 Output Voltage and Output Current of TEGs with Non-spin-coated PEDOT:PSS

The TEG module with five PEDOT:PSS layers exhibited both the highest output voltage and output current, mainly because it had the largest volume of PEDOT:PSS particles. Therefore, it was assumed that further increasing the volume of PEDOT:PSS might potentially boost its output voltage and output current. According to Table 4.3, the TEG module made with 100  $\mu\text{L}$  PEDOT:PSS (direct deposition, non-spin-coated) could produce a maximum output voltage of 0.545 V when subjected to a temperature gradient of 150  $^{\circ}\text{C}$ . In previous section, the highest temperature gradient was restrained to 120  $^{\circ}\text{C}$ . Here, the ceiling of temperature gradient was further pushed to observe the outputs of TEGs in this extreme temperature.

Similarly, its output voltage also depicted a proportional relationship with temperature gradient. For instance, when the temperature gradient increased from 0  $^{\circ}\text{C}$  to 150  $^{\circ}\text{C}$ , the average output voltage exalted from -5.092 mV to 453.556 mV. However, the output voltage of previous TEG with five layers of spin-coated PEDOT:PSS was more favourable. For instance, it recorded an average output voltage of 0.5181 V when the temperature gradient was only 120  $^{\circ}\text{C}$  but this TEG with non-spin-coated PEDOT:PSS only shown an average output voltage of 0.297 V at the same temperature gradient. The experimental setup is shown in Figure 4.8. Note that one side of the TEG is hanging in the air which served as cold side. Another side is stabilized by a weight on the hotplate which served as hot side.

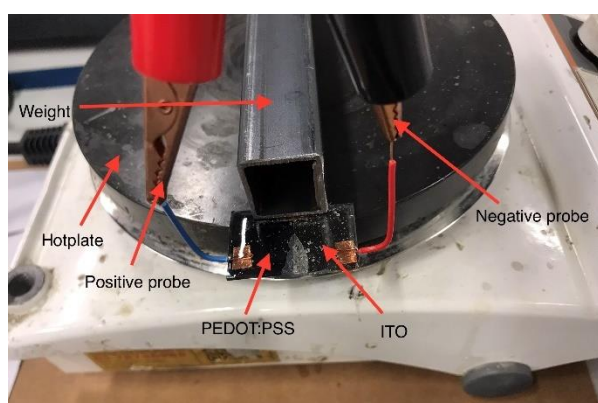


Figure 4.8: Experimental Setup to Characterize TEG (PEDOT:PSS Non-spin-coated).

Table 4.3: Output Voltage of a TEG (PEDOT:PSS Non-spin-coated).

Temperature Gradient	Output Voltage (mV)					
	Minimum	First quartile	Median	Third quartile	Maximum	Mean
0°C	-36.402	-18.459	-2.920	12.073	20.523	-5.092
10°C	-79.938	-25.594	63.964	147.870	216.907	62.643
20°C	-101.325	-63.092	15.230	119.002	157.794	23.958
30°C	-57.386	5.047	78.957	170.753	208.841	84.496
40°C	-178.768	-87.498	-20.736	68.428	162.084	-8.809
50°C	-54.690	4.365	74.701	178.788	235.968	86.881
60°C	-55.968	4.212	73.895	179.022	236.104	86.998
70°C	-135.205	20.663	82.801	177.379	277.262	93.811
80°C	-37.332	93.466	128.008	151.204	174.944	118.456
90°C	-84.763	11.016	49.507	90.984	129.352	50.524
100°C	-85.094	30.292	73.295	121.490	161.631	73.489
110°C	-13.293	198.147	247.690	295.726	354.558	240.639
120°C	12.766	258.029	305.843	346.551	398.751	297.355
130°C	22.854	322.590	367.275	432.173	465.882	372.626
140°C	165.591	357.159	388.861	485.845	502.932	412.186
150°C	129.334	416.928	444.171	503.824	544.733	453.556

Figure 4.9 shows the relationship between temperature gradient and the output voltage of the TEG module with non-spin-coated PEDOT:PSS. It could be observed that when the temperature gradient fell below 110 °C, the output voltage still fluctuated between positive and negative values. In contrast, when the temperature gradient reached 110 °C and above, the TEG module only generated positive voltage which would be more meaningful in real-life application.

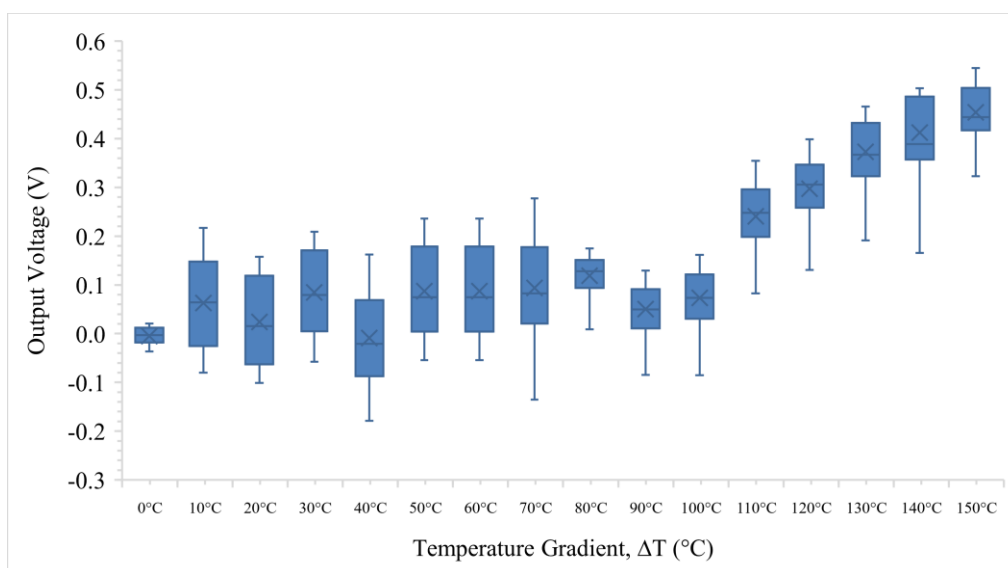


Figure 4.9: Output Voltage vs Temperature Gradient (PEDOT:PSS Non-spin-coated).

Although the output voltage of the TEG module with non-spin-coated PEDOT:PSS could reach a maximum value of around 0.5 V, its output current was exceptionally low. As shown in Table 4.4, this TEG module only recorded 19.4 nA as its highest output current when subjected to a temperature gradient of 150 °C. In fact, the previously reported TEG module with five layers of spin-coated PEDOT:PSS even had greater output current (max. 62.66 nA @ 120 °C temperature gradient). Furthermore, its output current oscillated between positive value and negative value when the temperature gradient was set below 140 °C. This oscillation could hardly be meaningful to any actual application. The t-TEG can only produce reasonable positive output current when the temperature gradient was 140 °C and above.

Table 4.4: Output current of a single TEG (PEDOT:PSS non-spin-coated).

Temperature Gradient	Output Current (nA)					
	Minimum	First quartile	Median	Third quartile	Maximum	Mean
0°C	-10.139	-7.292	-0.950	7.566	10.240	-0.115
10°C	-9.780	-7.478	-1.945	7.365	9.870	-0.055
20°C	-8.877	-6.197	1.381	6.169	8.983	0.044
30°C	-8.855	-5.991	0.036	6.645	8.920	-0.091
40°C	-8.817	-6.627	2.793	6.823	8.893	0.199
50°C	-8.859	-6.864	-1.693	6.263	8.960	-0.384
60°C	-8.254	0.056	0.088	0.114	8.216	0.035
70°C	-8.169	-6.393	1.691	6.286	8.681	0.212
80°C	-7.890	-5.880	-2.140	5.940	8.930	-0.106
90°C	-7.501	-5.739	0.562	7.304	9.379	0.535
100°C	-6.901	-4.990	1.746	7.296	9.957	1.148
110°C	-5.821	-3.435	3.489	9.069	10.912	3.067
120°C	-4.288	-2.364	6.301	10.870	12.446	4.977
130°C	-2.172	1.648	5.871	11.530	15.171	6.405
140°C	0.346	3.554	9.942	14.628	17.839	9.321
150°C	3.120	5.865	10.500	16.700	19.400	11.182

Figure 4.10 illustrates the relationship between output current and temperature gradient across the TEG module with non-spin-coated PEDOT:PSS. When the temperature gradient fell below 90 °C, the average output current was roughly zero. On the other hand, when the temperature gradient escalated from 90 °C to 150 °C, the average output current stably increased. However, the TEG only stopped producing negative output current when the temperature gradient reached 140 °C or above. This could be due to the excessive PEDOT:PSS created too many holes as compared to the amount of free electrons from the ITO. The free electrons might move directly from ITO to PEDOT:PSS through the copper tape instead of passing through the jumper wire and electrometer. This created a conflict with the originally planned direction of electrons flow.

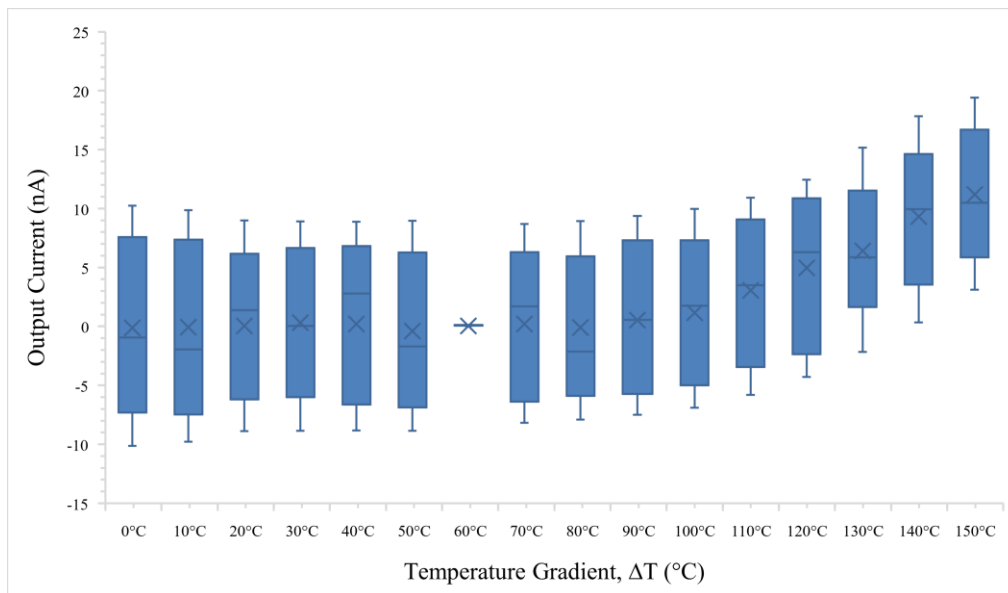


Figure 4.10: Output Current vs Temperature Gradient (PEDOT:PSS Non-spin-coated).

#### 4.4 TEGs with Non-spin-coated PEDOT:PSS Connected in Series

Since the TEG with non-spin-coated PEDOT:PSS required only around 1 hour to be fabricated, as compared to the one with spin-coated PEDOT:PSS which fabrication could take up to 4 hours. Making more TEGs with non-spin-coated PEDOT:PSS and study their behaviour in series and in parallel might discover something meaningful. The output voltage and output current of five TEGs (PEDOT:PSS non-spin-coated) connected in series and nine TEGs (PEDOT:PSS non-spin-coated) connected in series are tabulated in Table 4.5.

When nine TEGs were connected in series, it could output the maximum voltage of 1.163 V under a temperature gradient of 150 °C, while the five TEGs connected in series could only produce 0.782 V for the same temperature gradient. On the contrary, five TEGs connected in series recorded a higher output current of 14.879 nA under a temperature gradient of 150 °C, while nine TEGs connected in series only stood at 1.260 nA. In a nutshell, there existed a trade-off between output voltage and output current, when TEGs were connected in series. The experimental setup is shown in Figure 4.11. Note that one side of the TEG is hanging in the air which served as cold side. Another side is stabilized by a weight on the hotplate which served as hot side.

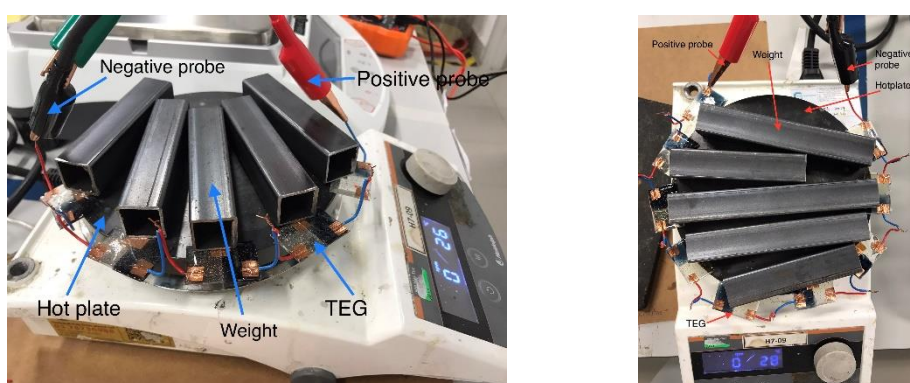


Figure 4.11: Five TEGs Connected in Series (Left) and Nine TEGs Connected in Series (Right).

Table 4.5: Output Voltage and Output Current of Five TEGs and Nine TEGs, Both Connected in Series and PEDOT:PSS Non-spin-coated.

Temperature Gradient, $\Delta T$ (°C)	Average output voltage (V)		Average output current (nA)	
	5 TEGs	9 TEGs	5 TEGs	9 TEGs
0°C	-0.013	-0.014	-1.935	2.003
10°C	-0.001	0.016	-0.168	-1.350
20°C	-0.012	0.007	-0.124	-0.745
30°C	0.001	0.081	0.738	-0.003
40°C	0.005	0.118	0.096	0.000
50°C	0.112	0.282	1.586	0.003
60°C	0.185	0.487	-0.951	-0.003
70°C	0.058	0.727	-0.419	0.009
80°C	0.125	0.855	-2.312	0.853
90°C	0.087	0.881	0.143	0.225
100°C	0.112	0.964	0.232	0.119
110°C	0.205	1.031	1.139	0.856
120°C	0.520	1.076	-0.357	0.166
130°C	0.633	1.063	7.130	1.860
140°C	0.663	1.101	10.543	0.356
150°C	0.782	1.163	14.879	1.260

The effect of the number of TEGs connected in series on the output voltage and output current was observed in Figure 4.12 where the dotted lines represent output voltage and the solid lines represent output current. The outputs from five TEGs connected in series are elucidated by green colour, while the outputs from nine TEGs connected in series are elucidated by orange colour. It displays an inverse proportion between the number of TEGs connected in series and its output current. Although higher output voltage could be achieved by adding more TEGs in series, it limits the output current.

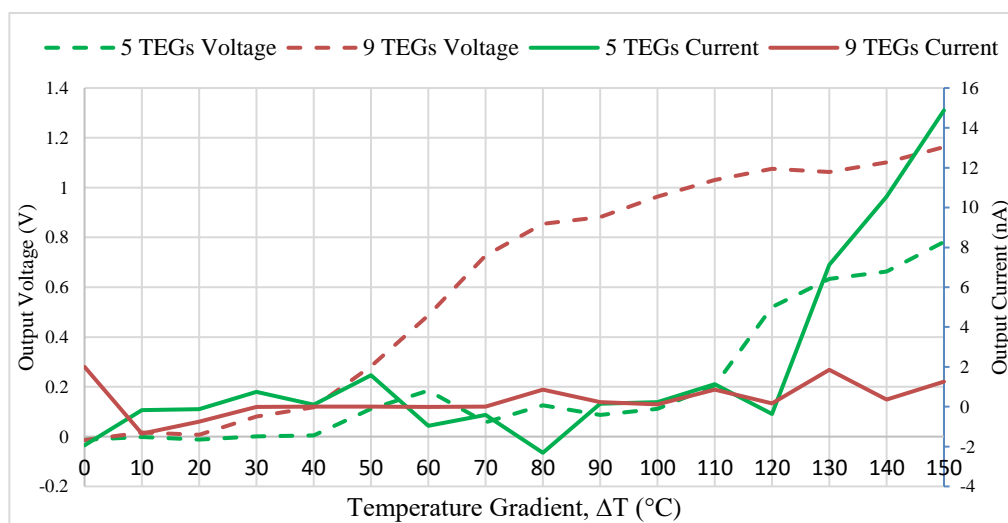


Figure 4.12: Outputs of Five TEGs in Series vs Nine TEGs in Series (PEDOT:PSS Non-spin-coated).

#### 4.5 TEGs with Non-spin-coated PEDOT:PSS Connected in Parallel

The output voltage and output current of five TEGs / nine TEGs connected in series were studied in previous section. For completeness, it is also worth examining the output of these TEGs in the parallel configuration. The output voltage and output current of five TEGs connected in parallel were shown in Table 4.6 where the temperature gradient across these five TEGs was ranged from 0 °C until 150 °C. Figure 4.14 and Figure 4.15 were also plotted to illustrate the relationship between output voltage and temperature gradient; output current and temperature gradient respectively. The experimental setup was shown in Figure 4.13. Note that one side of the TEG is hanging in the air which served as cold side. Another side is stabilized by a weight on the hotplate which served as hot side.



Figure 4.13: Five TEGs Connected in Parallel.

Table 4.6: Output Voltage and Output Current of Five TEGs in parallel.

Temperature gradient, $\Delta T$ ( $^{\circ}\text{C}$ )	Average Output Voltage (V)	Average Output Current (nA)
0 $^{\circ}\text{C}$	0.000	0.121
10 $^{\circ}\text{C}$	0.000	0.832
20 $^{\circ}\text{C}$	0.000	1.169
30 $^{\circ}\text{C}$	-0.001	-0.110
40 $^{\circ}\text{C}$	0.001	0.050
50 $^{\circ}\text{C}$	0.003	0.731
60 $^{\circ}\text{C}$	0.001	0.670
70 $^{\circ}\text{C}$	0.001	0.144
80 $^{\circ}\text{C}$	0.004	2.516
90 $^{\circ}\text{C}$	0.006	-0.032
100 $^{\circ}\text{C}$	0.028	0.653
110 $^{\circ}\text{C}$	0.036	3.171
120 $^{\circ}\text{C}$	0.051	2.938
130 $^{\circ}\text{C}$	0.184	3.439
140 $^{\circ}\text{C}$	0.290	6.442
150 $^{\circ}\text{C}$	0.290	10.557

According to Figure 4.14, the output voltages were close to zero when the temperature gradient across five TEGs fell below 100°C. It started to spike from 0.028 V to 0.290 V after the temperature gradient rose from 100°C to 150°C. Comparing these five TEGs connected in parallel with a single TEG (PEDOT:PSS non-spin-coated), their output voltages were relatively lower. For instance, when the temperature gradient was 150°C, a single TEG (PEDOT:PSS non-spin-coated) could produce an average output voltage of 0.454 V while these five TEGs connected in parallel could only produce an average output voltage of 0.29 V. This might be due to the wire connection (increase in wire length and solder) which induced voltage drop. Another possibility might lie on the TEGs themselves which could be referred to uneven PEDOT:PSS spread on the glass substrate, degradation of PEDOT:PSS in room temperature (they were left in room temperature more than 12 hours and left overnight in refrigerator before testing to collect data for the study), or improper connection between PEDOT:PSS and copper tape or ITO and copper tape or both, during fabrication. Despite that, it still exhibited a positive relationship between the output voltage and temperature gradient.

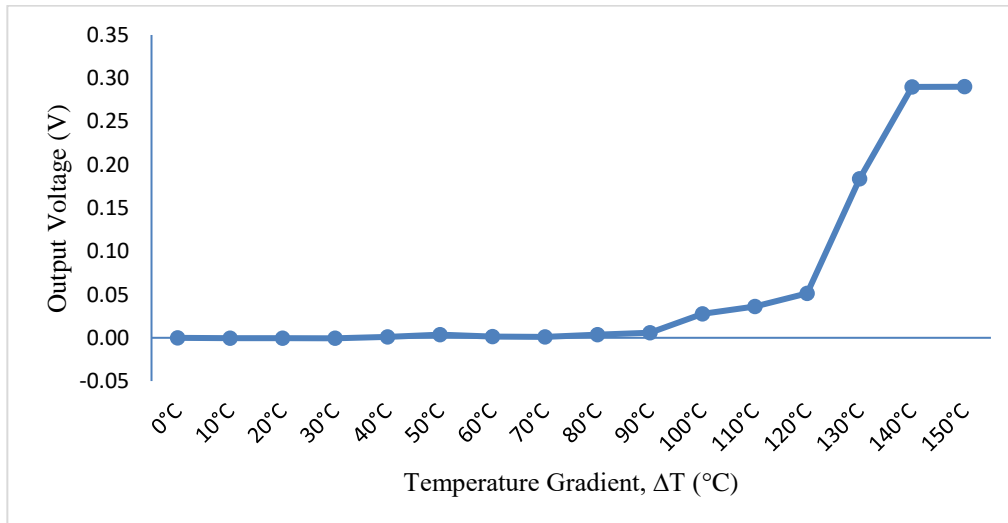


Figure 4.14: Output Voltage of Five TEGs in Parallel (PEDOT:PSS Non-spin-coated)

Figure 4.15 shows the average output current of five TEGs connected in parallel when subjected to a set of temperature gradients ranged from 0 °C until 150 °C. It was observed that the output current fluctuated between zero when the temperature gradient was set below 100°C. It only shown a relatively stable uphill trend when the temperature gradient was set 100°C and above. However, after connecting five TEGs in parallel, it does not seem to have any improvement on the output current. For instance when the temperature gradient was set at 150°C, a single TEG (PEDOT:PSS non-spin-coated) recorded an average output current of 11.182 nA while five TEGs (PEDOT:PSS non-spin-coated) could only produce an average output current of 10.557 nA. Theoretically, connecting TEGs in parallel should yield a higher output current but this expectation was not observed in this case. Again, this phenomenon could be explained by a few factors. Firstly, since the wire used to connect TEGs in parallel was longer, it served as an extra resistance for the current to flow and also introduced voltage drop. On the other hand, it might due to the TEGs themselves as well which included improper connection, uneven spread of PEDOT:PSS or degradation of PEDOT:PSS over time. Nevertheless, the overall output current also displayed a growing trend when the temperature gradient across them was increased.

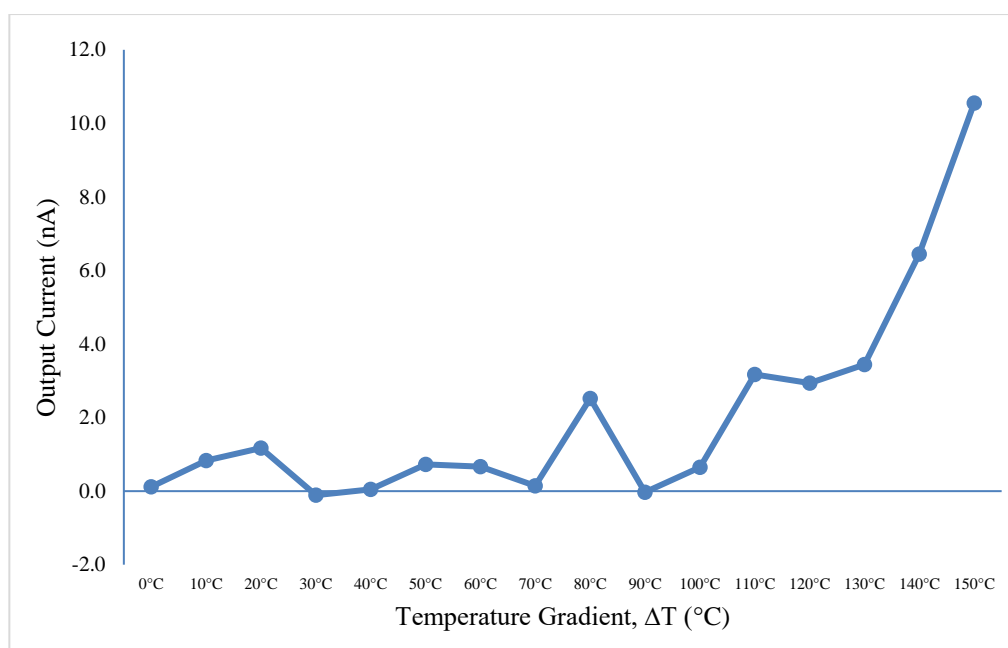


Figure 4.15: Output Current of Five TEGs in Parallel (PEDOT:PSS Non-spin-coated)

#### 4.6 Output Power of All TEGs

The output power from all TEGs could be calculated by multiplying its output voltage by its output current. Therefore, the output powers of the TEGs of different PEDOT:PSS layers (from 1 layer to 5 layers), TEG with non-spin-coated PEDOT:PSS, five TEGs (PEDOT:PSS non-spin-coated) connected in series, five TEGs (PEDOT:PSS non-spin-coated) connected in parallel and nine TEGs (PEDOT:PSS non-spin-coated) connected in series could be mathematically determined. The primary purpose of calculating output power was to determine which PEDOT:PSS configuration could produce the highest output power. By knowing that configuration, further experiments could be executed such as adding additive into PEDOT:PSS to further boost up its outputs. Table 4.7 summarizes the computed output powers of all TEGs in this research project.

Table 4.7: Average Output Power of all TEGs.

Temperature Gradient, $\Delta T$ (°C)	Average output power (nW)								
	PEDOT:PSS spin-coated					PEDOT:PSS non-spin-coated			
	TEG (1 layers)	TEG (2 layers)	TEG (3 layers)	TEG (4 layers)	TEG (5 layers)	TEG	5 TEGs in series	9 TEGs in series	5 TEGs in parallel
0°C	0.0013	0.0000	0.0003	0.0519	0.2028	0.0006	0.0252	0.0280	0.0000
10°C	0.0001	0.0002	0.0011	0.0129	0.0438	0.0034	0.0002	0.0216	0.0000
20°C	0.0000	0.0010	0.0016	0.0050	0.4305	0.0011	0.0015	0.0052	0.0000
30°C	0.0000	0.0013	0.0051	0.0105	0.6430	0.0077	0.0007	0.0002	0.0001
40°C	0.0001	0.0016	0.0090	0.0128	0.7601	0.0018	0.0005	0.0000	0.0001
50°C	0.0000	0.0034	0.0131	0.0137	1.0697	0.0334	0.1776	0.0008	0.0022
60°C	0.0001	0.0074	0.0158	0.0239	1.4448	0.0030	0.1759	0.0015	0.0007
70°C	0.0000	0.0316	0.0216	0.0969	1.7192	0.0199	0.0243	0.0065	0.0001
80°C	0.0000	0.0327	0.0218	0.1073	16.6327	0.0126	0.2890	0.7293	0.0101
90°C	0.0000	0.0415	0.0342	0.2733	17.8122	0.0270	0.0124	0.1982	0.0002
100°C	0.0193	0.1404	0.1277	0.8944	24.3318	0.0844	0.0260	0.1147	0.0183
110°C	0.0197	0.1671	0.2512	1.0052	28.0575	0.7380	0.2335	0.8825	0.1142
120°C	0.0230	0.2724	0.5410	2.2536	32.4641	1.4799	0.1856	0.1786	0.1498
130°C						2.3867	4.5133	1.9772	0.6328
140°C						3.8420	6.9900	0.3920	1.8682
150°C						5.0717	11.6354	1.4654	3.0615

Remark: The highest output power recorded among all TEGs tested was highlighted in brown colour.

From Table 4.7, it could be seen that when the number of PEDOT:PSS layers increased from one layer to five layers, the output power rose as well. It might be due to the increasing abundance of the PEDOT:PSS particles which made the t-TEGs to become more conductive and also more free holes to accept electrons from ITO. On the other hand, the TEG with non-spin-coated PEDOT:PSS produced lesser output power as compared to the TEG with five layers of spin-coated PEDOT:PSS. This implied that excessive PEDOT:PSS does not necessarily be beneficial to the performance of a TEG. It might have adverse effects and also created PEDOT:PSS wastage. Lastly, although the TEGs connected in series had highest output voltage, they had relatively small output power mainly due to relatively low output current. Connecting TEGs in series significantly enlarged the overall resistance and small output power was therefore expected. In addition, connecting five TEGs (PEDOT:PSS non-spin-coated) in parallel shown a poorer output power as compared to the five TEGs (PEDOT:PSS non-spin-coated) connected in series. For instance, when the temperature was 150 °C, five TEGs connected in series prompted an output power of 11.6354 nW while five TEGs connected in parallel only gave 3.0615 nW. This verified the configuration of commercially available opaque Peltier cell which also connected all its thermocouple in series (Sole, 2020).

The commercially available ultra-low power LED required a forward voltage of 1.8 V and a current of 2 mA to turn on itself, which was equivalent to  $1.8 \text{ V} \times 2 \text{ mA} = 3.6 \text{ mW}$  (Digi-Key Electronics, 2022). Even taking the highest output power (32.4641 nW) from the t-TEG throughout this research project, it was still approximately 100,000 times lesser than the required power to turn on the ultra-low power LED. The TEG required a tremendous improvement by making changes in additive, materials selection, or morphology. However, the TEG made in this project had only a dimension of 30 mm  $\times$  20 mm which only equivalent to 0.0006 m<sup>2</sup>. By pairing more TEGs (5 layers spin-coated PEDOT:PSS) in series and changes its morphology and additives, it was believed to have improvement in overall output power.

#### 4.7 Accuracy of Keithley 6514 System Electrometer

In fact, the high output voltage but low output current of all tested TEGs first doubted the accuracy of the electrometer. It was thought that the electrometer was not properly calibrated or simply because the heat from the hotplate affected the electrometer's accuracy and induced it to yield high voltage reading on its LCD display. In order to justify its reliability, its positive probe (red colour) and negative probe (black colour) were hung approximately 10 mm above the hotplate and the hotplate was then heated from room temperature (26 °C) up to 176 °C (as shown in Figure 4.16). The voltage readings on the electrometer were then tabulated in Table 4.8.

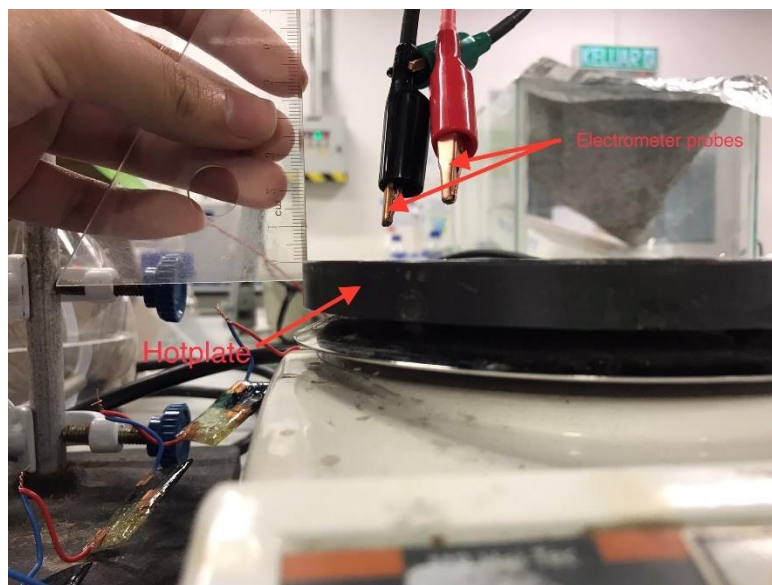


Figure 4.16: Both Positive Probe and Negative Probe Were Placed Approximately 10 mm Above the Hotplate Which Temperature Rose from 26 °C to 176 °C.

According to Table 4.8, as the temperature of the hotplate increased, the electrometer's voltage reading fluctuated around 0.0125 V with insignificant trend of rising voltage. This small voltage variance (noise) could not contribute to the high output voltages that were detected in previously reported TEGs. This justified that the electrometer's accuracy was not substantially influenced by the heat emitted from the hotplate. Moreover, the current readings were also substantially small in pico-Ampere range. This small current variance did not nullify the previous current data recorded in nano-Ampere range. Figure 4.17 was plotted to illustrate the relationship between the electrometer voltage readings and the hotplate temperature. In addition, Figure 4.18 demonstrates the relationship between the electrometer current readings and the hotplate temperature.

Table 4.8: Rising Hotplate Temperature Only Resulted in Negligibly Small Voltage Reading on The Electrometer.

Hotplate Temperature (°C)	Voltage Reading on the Electrometer (V)	Current Reading on the Electrometer (pA)
26	0.0084	-57.408
36	0.0077	0.513
46	0.0103	0.156
56	0.0124	-0.512
66	0.0116	-1.637
76	0.0106	0.137
86	0.0130	-0.199
96	0.0152	-0.619
106	0.0148	0.569
116	0.0118	-0.375
126	0.0163	-0.053
136	0.0196	0.098
146	0.0192	-0.826
156	0.0158	-0.920
166	0.0166	-0.465

As shown in Figure 4.17 and Figure 4.18, The electrometer shown a voltage reading of 0.0084 V / current reading of -57.408 pA at room temperature (26 °C) and increased to 0.0166 V / -0.465 pA when the hotplate temperature was set at 166 °C. Although the electrometer meter did not show 0.0000 V / 0.0000 pA along the heating process but these small initial voltage / current readings did not nullify the voltage / current data obtained previously which most of them fell on 0.1 V / 0.1 nA or above.

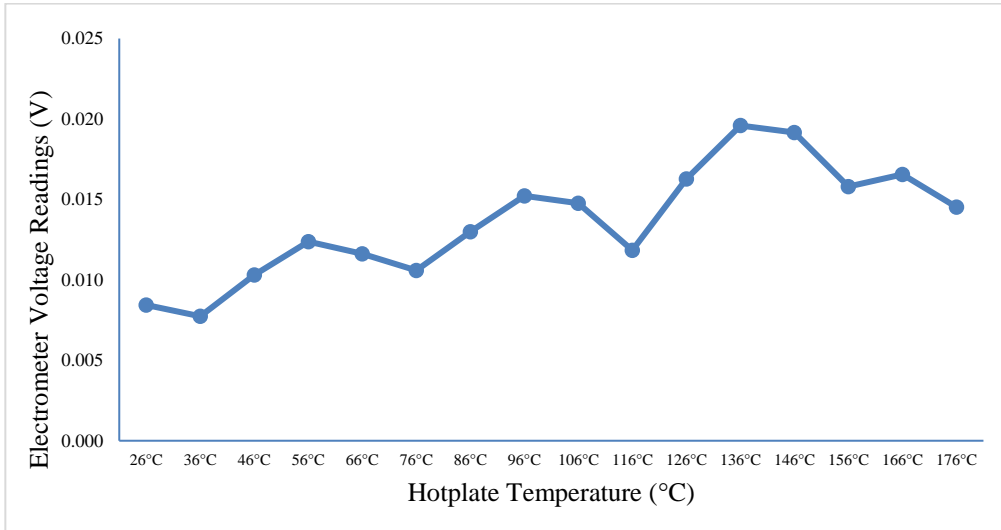


Figure 4.17: Electrometer Voltage Reading vs Hotplate Temperature.

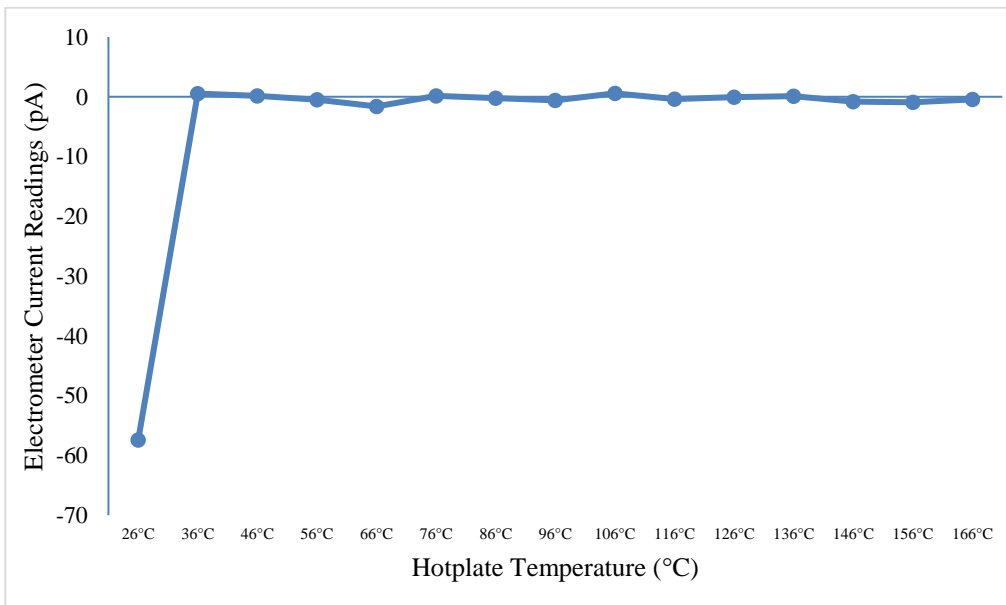
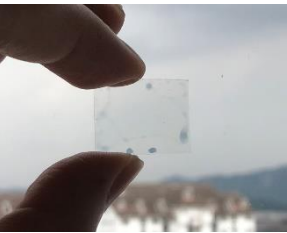


Figure 4.18: Electrometer Current Reading vs Hotplate Temperature.

#### 4.8 Transparency of PEDOT:PSS Thin Layers

Table 4.9 shows the transparency of six PEDOT:PSS coated glass substrates. Each PEDOT:PSS layer was deposited by dropping 70  $\mu\text{L}$  PEDOT:PSS solution on a 15 mm  $\times$  20 mm glass substrate, placed on a spin coater machine. Clearly, the more PEDOT:PSS layers coated on the glass substrate, the lower its transparency.

Table 4.9: Transparency of Glass Substrate with Different PEDOT:PSS Layers.

		
1 layer of PEDOT:PSS	2 layers of PEDOT:PSS	3 layers of PEDOT:PSS
		
4 layers of PEDOT:PSS	5 layers of PEDOT:PSS	100 $\mu\text{L}$ PEDOT:PSS (non-spin-coated)

The respective % transmittance of clear glass substrate, 3, 4 and 5 PEDOT:PSS layers coated glass substrate was shown in Figure 4.19. The visible spectrum wavelength fell between 400 nm (violet) and 800 nm (red). The clear glass substrate mostly attained 100% transparency across the visible spectrum while the % transparency of PEDOT:PSS coated glass substrate started to decrease, as the number of PEDOT:PSS layers increased. However, even the number of PEDOT:PSS layers climbed to 5 layers, its transparency still fell above 80 % threshold within visible spectrum. This fulfilled one of the objectives to ensure the thermoelectric generators were transparent, enabling it to be utilized in various fields such as imperceptible robotics, sensors and wearables.

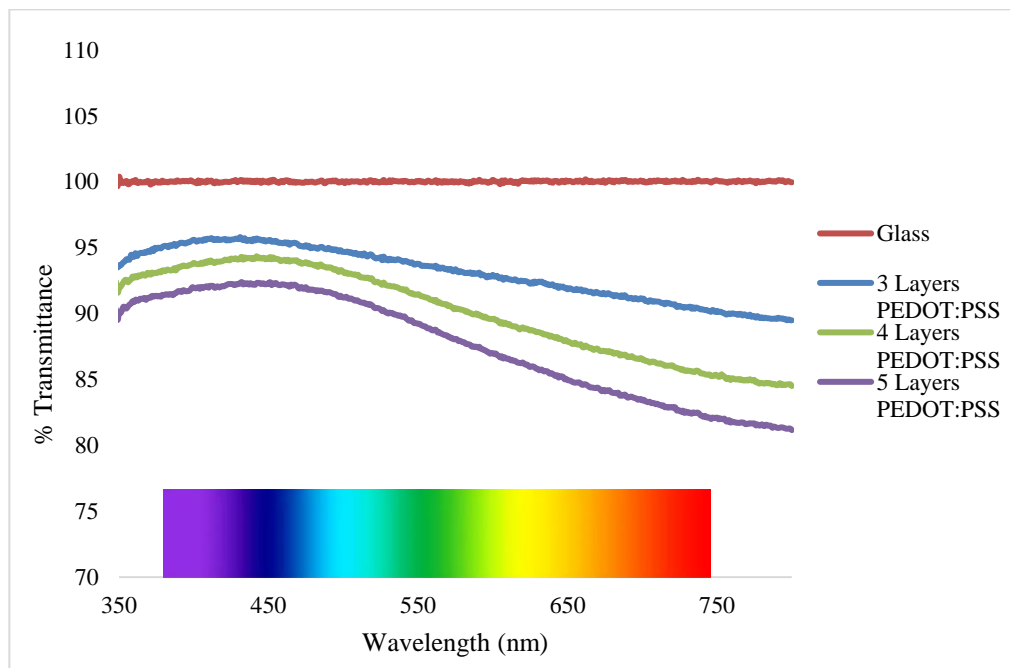
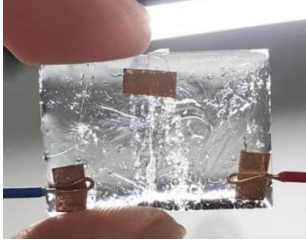
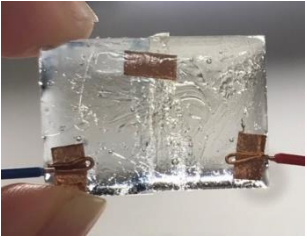
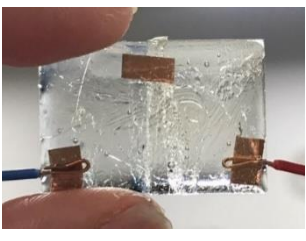
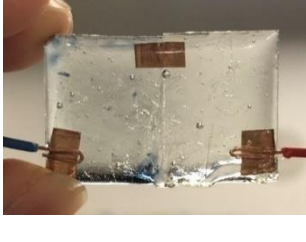
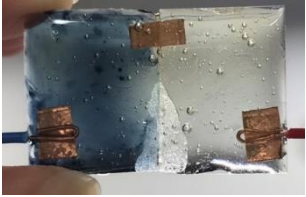


Figure 4.19: % Transmittance of Glass Substrate and Glass Substrate with Different Layers of PEDOT:PSS.

#### **4.9 Effect of High Temperature on the Transparency of t-TEGs**

There was a layer of clear epoxy coated on each TEG. It functions as a shield to protect both ITO and PEDOT:PSS from moisture, scratch, dust and dirt. However, this clear epoxy layer turned yellow when exposed to high temperature especially for extended period. This phenomenon was known as discoloration or ambering (Felix, J., 2021). Discoloration of epoxy could be observed on those t-TEGs during experiment when they were subjected to temperature roughly above 120 °C. Their epoxy even turned yellowed within a matter of seconds when placed above hotplate which temperature was set higher. This discoloration could be observed by bare eyes, and it certainly made the t-TEGs became less transparent as the colour grew darker. As a result, those clear epoxy coated t-TEGs would permanently lose their transparency if exposed to high temperature, making the t-TEGs no longer transparent. This restrained t-TEGs to be implemented in high temperature environment. Moreover, not only high temperature could result in epoxy discoloration but also exposure to UV light, moisture and oxidation for an extended period. Table 4.10 illustrates some examples of t-TEGs before and after heated from 26 °C to 176 °C. The yellowish region might not be clearly captured in the following pictures, but the discoloration definitely appeared more obviously when observed with bare eyes.

Table 4.10: Discoloration of Clear Epoxy After Exposure to High Temperature.

Before heating	After heating to 176 °C for 30 seconds	After heating to 176 °C for 1 minute
t-TEG with 2 layers of PEDOT:PSS		
		
t-TEG with 5 layers of PEDOT:PSS		
		
TEG with non-spin-coated PEDOT:PSS		
		

#### 4.10 Summary

There were more than 40 TEGs fabricated throughout the entire experiment as shown in Figure 4.20. The TEGs were coated with a layer of clear epoxy to protect PEDOT:PSS and ITO from moisture, dirt, and to strengthen the connection of jumper wire terminals. The % transmittance of all TEGs with spin-coated TEG fell above 80 % threshold and it was found that TEG with five layers of PEDOT:PSS thin film could produce the maximum output power of 32.4614 nW under a temperature gradient of 120 °C. Moreover, 100  $\mu$ L of PEDOT:PSS solution was also being directly deposited onto glass substrate and later paired with ITO coated glass to form thermocouple. It was found that although its output voltage was as high as the TEG with five layers of spin-coated PEDOT:PSS, its output current was significantly lower. For all TEGs with non-spin-coated PEDOT:PSS, the highest output power recorded was only 11.6354 nW under a temperature gradient of 150 °C. This output power was approximately three times smaller than the TEG with five layers of PEDOT:PSS spin-coated. The final verdict pointed out that the TEG with five layers of PEDOT:PSS thin film exhibited the greatest output performance among all.



Figure 4.20: Some Samples of Fabricated TEGs.

## CHAPTER 5

### CONCLUSIONS AND RECOMMENDATIONS

#### 5.1 Conclusions

This research project commenced on 31 January 2022 and ended on 12 September 2022. The entire project aimed to fabricate a transparent thermoelectric generator (t-TEG) under UTAR Sungai Long Campus laboratory setting. The first part of the project primarily focused on literature review to understand the working principle of a transparent thermoelectric generator and to select two materials that could be paired as thermocouple which gave the highest output power. It was then concluded that PEDOT:PSS as p-type material and ITO as n-type could yield the highest output power among all other research studied. The second part of the project focused on fabricating the transparent thermoelectric generator using spin-coating method and direct deposition method. The fabricated TEGs were then characterized and their output parameters were analysed. The highest output power was recorded at 32.4614 nW when a temperature gradient of 120 °C was subjected to the t-TEG with 5 layers of spin-coated PEDOT:PSS. The well-documented methodology could be served as a valuable guidance for upcoming scholars to conduct more experiments on this field of transparent thermoelectric generator.

#### 5.2 Recommendations for Future Work

This research project required knowledge from multifold disciplines such as material science, chemistry, electrical and electronic engineering. Instead of making this as an individual research project, one can consider transforming this project to a group effort consisted of students from different disciplines. In addition, it would be great if the researcher had initial hands-on experience on the spin-coating method because it would save a significant amount of time if spin-coating method was mastered beforehand. Lastly, the chemical TFMS which was used by Wang et al. (2020) to treat PEDOT:PSS to improve its Seebeck coefficient was not readily available in UTAR inventory. Consider purchasing this chemical might help in getting a higher output power.

## REFERENCES

- Al-Tahaine, H. and AlEsa, A.H.M., 2022. A hybrid TEG/evacuated tube solar collectors for electric power generation and space heating. *Journal of Engineering and Applied Science*, [online] 69(1), pp.1–15. <https://doi.org/10.1186/S44147-021-00065-1/FIGURES/15>.
- Bastiaansen, C., Schmidt, H.W., Nishino, T. and Smith, P., 1993. Transparency and dichroism of ultra-drawn UHMW-PE films in the visible wavelength range. *Polymer*, 34(18), pp.3951–3954. [https://doi.org/10.1016/0032-3861\(93\)90526-G](https://doi.org/10.1016/0032-3861(93)90526-G).
- Boverhof, D.R., Bramante, C.M., Butala, J.H., Clancy, S.F., Lafranconi, W.M., West, J. and Gordon, S.C., 2015. Comparative assessment of nanomaterial definitions and safety evaluation considerations. *Regulatory Toxicology and Pharmacology*, 73(1), pp.137–150. <https://doi.org/10.1016/j.yrtph.2015.06.001>.
- Buonomenna, M.G., 2016. Smart composite membranes for advanced wastewater treatments. *Smart Composite Coatings and Membranes: Transport, Structural, Environmental and Energy Applications*, pp.371–419. <https://doi.org/10.1016/B978-1-78242-283-9.00014-2>.
- Carlander, D. and Skentelbery, C., 2021. *EU Regulations and Nanotechnology Innovation. Molecular and Integrative Toxicology*. [https://doi.org/10.1007/978-3-030-79808-6\\_8](https://doi.org/10.1007/978-3-030-79808-6_8).
- Chen, X., Hu, Y., Xie, Z. and Wang, H., 2018. Materials and Design of Photocatalytic Membranes. *Current Trends and Future Developments on (Bio-) Membranes: Photocatalytic Membranes and Photocatalytic Membrane Reactors*, pp.71–96. <https://doi.org/10.1016/B978-0-12-813549-5.00003-7>.
- Coroa, J., Morais Faustino, B.M., Marques, A., Bianchi, C., Koskinen, T., Juntunen, T., Tittonen, I. and Ferreira, I., 2019. Highly transparent copper iodide thin film thermoelectric generator on a flexible substrate. *RSC Advances*, 9(61), pp.35384–35391. <https://doi.org/10.1039/C9RA07309D>.
- Denchak, M., 2018. *Fossil fuels: the dirty facts*. [online] Available at: <<https://www.nrdc.org/stories/fossil-fuels-dirty-facts>> [Accessed 21 April 2022]
- Digi-Key Electronics, 2022. *LED indication – discreate: SunLED XZCM2CRK53WA-8VF*. [online] Available at: <<https://www.digikey.com/en/products/detail/sunled/XZCM2CRK53WA-8VF/10449772>> [Accessed 4 September 2022].

Ding, Y., Qiu, Y., Cai, K., Yao, Q., Chen, S., Chen, L. and He, J., 2019. High performance n-type Ag<sub>2</sub>Se film on nylon membrane for flexible thermoelectric power generator. *Nature Communications*, 10(1). <https://doi.org/10.1038/s41467-019-08835-5>.

Dong, L., Zhu, G.S., Xu, H.R., Jiang, X.P., Zhang, X.Y., Zhao, Y.Y., Yan, D.L., Yuan, L. and Yu, A.B., 2019. Preparation of indium tin oxide (ITO) thin film with (400) preferred orientation by sol-gel spin coating method. *Journal of Materials Science: Materials in Electronics*. <https://doi.org/10.1007/s10854-019-01126-1>.

Enescu, D., 2019. Thermoelectric Energy Harvesting: Basic Principles and Applications. *Green Energy Advances*. <https://doi.org/10.5772/INTECHOPEN.83495>.

Felix, J., 2021. *Why epoxy resin turns yellow and how to prevent it*. [online] Available at: <https://lifespecialtycoatings.com/deep-dive-into-the-discoloration-of-epoxy-resin-over-time/> [Accessed 4 September 2022].

Ferreira, M., Loureiro, J., Nogueira, A., Rodrigues, A., Martins, R. and Ferreira, I., 2015. SnO<sub>2</sub> thin Film Oxides Produced by rf Sputtering for Transparent Thermoelectric Devices. *Materials Today: Proceedings*, 2(2), pp.647–653. <https://doi.org/10.1016/J.MATPR.2015.05.090>.

Fourati, N., Blel, N., Lattach, Y., Ktari, N. and Zerrouki, C., 2016. Chemical and Biological Sensors from Conducting and Semiconducting Polymers. *Reference Module in Materials Science and Materials Engineering*. <https://doi.org/10.1016/B978-0-12-803581-8.01733-1>.

Geisz, J.F., France, R.M., Schulte, K.L., Steiner, M.A., Norman, A.G., Guthrey, H.L., Young, M.R., Song, T. and Moriarty, T., 2020. Six-junction III–V solar cells with 47.1% conversion efficiency under 143 Suns concentration. *Nature Energy*, 5(4), pp.326–335. <https://doi.org/10.1038/s41560-020-0598-5>.

Hendricks, T.J. and Crane, D.T., 2012. *Thermoelectric energy recovery systems: Thermal, thermoelectric, and structural considerations. Modules, Systems, and Applications in Thermoelectrics*. <https://doi.org/10.1201/b11892>.

Inayat, S.B., Rader, K.R. and Hussain, M.M., 2014. Manufacturing of Thermoelectric Nanomaterials (Bi<sub>0.4</sub>Sb<sub>1.6</sub>Te<sub>3</sub>/Bi<sub>1.75</sub>Te<sub>3.25</sub>) and Integration into Window Glasses for Thermoelectricity Generation. *Energy Technology*, 2(3), pp.292–299. <https://doi.org/10.1002/ente.201300166>.

International Renewable Energy Agency, 2021. *Energy profile: Malaysia*. [pdf] United Arab Emirates: International Renewable Energy Agency. Available at: [https://www.irena.org/IRENADocuments/Statistical\\_Profiles/Asia/Malaysia\\_Asia\\_RE\\_SP.pdf](https://www.irena.org/IRENADocuments/Statistical_Profiles/Asia/Malaysia_Asia_RE_SP.pdf) [Accessed 20 April 2022]

Jamaludin, N., Mohammed, N.I., Khamidi, M.F. and Wahab, S.N.A., 2015. Thermal Comfort of Residential Building in Malaysia at Different Microclimates. *Procedia - Social and Behavioral Sciences*, 170, pp.613–623. <https://doi.org/10.1016/j.sbspro.2015.01.063>.

Jaziri, N., Boughamoura, A., Müller, J., Mezghani, B., Tounsi, F. and Ismail, M., 2020. A comprehensive review of Thermoelectric Generators: Technologies and common applications. *Energy Reports*, 6, pp.264–287. <https://doi.org/10.1016/J.EGYR.2019.12.011>.

Jouhara, H., Żabnieńska-Góra, A., Khordehgah, N., Doraghi, Q., Ahmad, L., Norman, L., Axcell, B., Wrobel, L. and Dai, S., 2021. Thermoelectric generator (TEG) technologies and applications. *International Journal of Thermofluids*, 9, p.100063. <https://doi.org/10.1016/J.IJFT.2021.100063>.

Kaltenbrunner, M., Sekitani, T., Reeder, J., Yokota, T., Kuribara, K., Tokuhara, T., Drack, M., Schwödiauer, R., Graz, I., Bauer-Gogonea, S., Bauer, S. and Someya, T., 2013. An ultra-lightweight design for imperceptible plastic electronics. *Nature*, [online] 499(7459), pp.458–463. <https://doi.org/10.1038/nature12314>.

Kimura, M., Aramaki, T., Ikeguchi, Y., Yamamoto, Y., Ito, R., Tamura, M., Matsuda, T. and Uenuma, M., 2022. Thermoelectric Generator using Amorphous Ga-Sn-O Thin-Film Device. Institute of Electrical and Electronics Engineers (IEEE).pp.1–5. <https://doi.org/10.1109/icce53296.2022.9730487>.

Kreyling, W.G., Semmler-Behnke, M. and Chaudhry, Q., 2010. A complementary definition of nanomaterial. *Nano Today*, 5(3), pp.165–168. <https://doi.org/10.1016/J.NANTOD.2010.03.004>.

Lee, J.H., Shin, G., Baek, J.Y. and Kang, T.J., 2021. An Electricity-Generating Window Made of a Transparent Energy Harvester of Thermocells. *ACS Applied Materials & Interfaces*, [online] 13(18), pp.21157–21165. <https://doi.org/10.1021/acsami.1c00164>.

Li, X., Zou, R., Liu, Z., Mata, J., Storer, B., Chen, Y., Qi, W., Zhou, Z. and Zhang, P., 2022. Deciphering the superior thermoelectric property of post-treatment-free PEDOT:PSS/IL hybrid by X-ray and neutron scattering characterization. *npj Flexible Electronics* 2022 6:1, [online] 6(1), pp.1–8. <https://doi.org/10.1038/S41528-022-00138-Y>.

Liao, W., Liu, X., Li, Y., Xu, X., Jiang, J., Lu, S., Bao, D., Wen, Z. and Sun, X., n.d. Transparent, stretchable, temperature-stable and self-healing ionogel-based triboelectric nanogenerator for biomechanical energy collection. [online] <https://doi.org/10.1007/s12274-021-3797-x>.

Liu, W., Ren, Z. and Chen, G., 2013. Nanostructured Thermoelectric Materials. *Springer Series in Materials Science*, [online] 182, pp.255–285. [https://doi.org/10.1007/978-3-642-37537-8\\_11](https://doi.org/10.1007/978-3-642-37537-8_11).

Loureiro, J., Neves, N., Barros, R., Mateus, T., Santos, R., Filonovich, S., Reparaz, S., Sotomayor-Torres, C.M., Wyczisk, F., Divay, L., Martins, R. and Ferreira, I., 2014. Transparent aluminium zinc oxide thin films with enhanced thermoelectric properties. *Journal of Materials Chemistry A*, 2(18), pp.6649–6655. <https://doi.org/10.1039/c3ta15052f>.

Lu, K., 2014. Materials in Energy Conversion, Harvesting, and Storage. *Materials in Energy Conversion, Harvesting, and Storage*, [online] 9781118889107, pp.1–429. <https://doi.org/10.1002/97811188892374>.

Ma, Z., Wei, J., Song, P., Zhang, M., Yang, L., Ma, J., Liu, W., Yang, F. and Wang, X., 2021. Review of experimental approaches for improving zT of thermoelectric materials. *Materials Science in Semiconductor Processing*, 121, p.105303. <https://doi.org/10.1016/J.MSSP.2020.105303>.

Makhlouf, A.S.H., 2011. Current and advanced coating technologies for industrial applications. *Nanocoatings and Ultra-Thin Films*, pp.3–23. <https://doi.org/10.1533/9780857094902.1.3>.

Malaysian Investment Development Authority, 2022. Renewable energy. [online] Available at: <<https://www.mida.gov.my/industries/services/green-technology/renewable-energy/>> [Accessed 21 April 2022]

Mcsweeney, R., 2020. *Methane emissions from fossil fuels “severely underestimated”*. [online] Available at: <<https://www.carbonbrief.org/methane-emissions-from-fossil-fuels-severely-underestimated>> [Accessed 21 April 2022]

Mehta, R., Min, M. and Kaul, A.B., 2020. Sol-gel synthesized indium tin oxide as a transparent conducting oxide with solution-processed black phosphorus for its integration into solar-cells. *Journal of Vacuum Science & Technology B*, 38(6), p.063203. <https://doi.org/10.1116/6.0000471>.

Morin, S.A., Shepherd, R.F., Kwok, S.W., Stokes, A.A., Nemiroski, A. and Whitesides, G.M., 2012. Camouflage and Display for Soft Machines. *Science*, 337, pp.828–832.

Morse, E., 2013. *Renewable energy*. [online] Available at: <<https://www.nationalgeographic.org/article/renewable-energy/2nd-grade/>> [Accessed 21 April 2022]

National Institute of Environmental Health Sciences, 2022. *Human health impacts of climate change*. [online] Available at <[https://www.niehs.nih.gov/research/programs/climatechange/health\\_impacts/index.cfm](https://www.niehs.nih.gov/research/programs/climatechange/health_impacts/index.cfm)> [Accessed 21 April 2022]

Nguyen, N.-T., 2012. Fabrication technologies. *Micromixers*, pp.113–161. <https://doi.org/10.1016/B978-1-4377-3520-8.00004-8>.

Noh, Y.J., Kim, S.S., Kim, T.W. and Na, S.I., 2014. Cost-effective ITO-free organic solar cells with silver nanowire–PEDOT:PSS composite electrodes via

a one-step spray deposition method. *Solar Energy Materials and Solar Cells*, 120(PART A), pp.226–230. <https://doi.org/10.1016/J.SOLMAT.2013.09.007>.  
Paras and Kumar, A., 2021. Anti-Wetting Polymeric Coatings. *Reference Module in Materials Science and Materials Engineering*. <https://doi.org/10.1016/B978-0-12-820352-1.00141-3>.

Prangnell, L., n.d. Visible Light-Based Human Visual System Conceptual Model.

Rafique, M., Tahir, M.B., Rafique, M.S., Safdar, N. and Tahir, R., 2020. Nanostructure materials and their classification by dimensionality. *Nanotechnology and Photocatalysis for Environmental Applications*, pp.27–44. <https://doi.org/10.1016/B978-0-12-821192-2.00002-4>.

Ribeiro, J.M., Correia, F.C., Rodrigues, F.J., Reparaz, J.S., Goñi, A.R. and Tavares, C.J., 2021. Transparent niobium-doped titanium dioxide thin films with high Seebeck coefficient for thermoelectric applications. *Surface and Coatings Technology*, 425, p.127724. <https://doi.org/10.1016/J.SURFCOAT.2021.127724>.

Ritchie, H., Roser, M. and Rosado, P., 2020. Fossil fuels. [online] Available at: <<https://ourworldindata.org/fossil-fuels#:~:text=The%20burning%20of%20fossil%20fuels%20for%20energy%20began,down%20by%20coal%2C%20oil%20and%20gas%20since%201800.>>> [Accessed 21 April 2022].

Rowe, D.M., 2012. *Modules, Systems, and Applications in Thermoelectrics*. Thermoelectrics and Its Energy Harvesting. [online] Boca Raton, FL: CRC Press. Available at: <<https://login.libezp2.utar.edu.my/login?url=https://search.ebscohost.com/login.aspx?direct=true&db=edsebk&AN=457352&site=eds-live&scope=site>>.

Saberi, Y. and Sajjadi, S.A., 2022. A comprehensive review on the effects of doping process on the thermoelectric properties of Bi<sub>2</sub>Te<sub>3</sub> based alloys. *Journal of Alloys and Compounds*, 904. <https://doi.org/10.1016/j.jallcom.2022.163918>.

Smith, R., Peters, C. and Inomata, H., 2013. Historical Background and Applications. *Supercritical Fluid Science and Technology*, 4, pp.175–273. <https://doi.org/10.1016/B978-0-444-52215-3.00004-0>.

Sole, R. 2020. *What is a Peltier Cell (Peltier Cell) and how it works*. [online] Available at: <<https://hardwaresfera.com/en/articulos/que-es-celula-peltier/>> [Accessed 5 September 2022]

Sun, Z., Zhu, M., Zhang, Z., Chen, Z., Shi, Q., Shan, X., Yeow, R.C.H. and Lee, C., 2021. Artificial Intelligence of Things (AIoT) Enabled Virtual Shop Applications Using Self-Powered Sensor Enhanced Soft Robotic Manipulator. *Advanced Science*, [online] 8(14), p.2100230. <https://doi.org/https://doi.org/10.1002/advs.202100230>.

Tan, Q., Yuan, L., Liang, G. and Gu, A., 2022. Flexible, transparent, strong and high dielectric constant composite film based on polyionic liquid coated silver nanowire hybrid. *Applied Surface Science*, 576. <https://doi.org/10.1016/j.apsusc.2021.151827>.

Tektronix, 2022. *Keithley electrometer series 6500 & 6430*. [online] Available at: <<https://www.tek.com/en/products/keithley/low-level-sensitive-and-specialty-instruments/electrometers>> [Accessed 25 August 2022].

U.S. Environmental Protection Agency, 2022. *The sources and solutions: fossil fuels*. [online] Available at: <<https://www.epa.gov/nutrientpollution/sources-and-solutions-fossil-fuels#:~:text=When%20fossil%20fuels%20are%20burned,referred%20to%20as%20nitrogen%20oxides.>> [Accessed 21 April 2022]

U.S. Energy Information Administration, 2021. *Electricity explained: how electricity is generated*. [online] Available at: <<https://www.eia.gov/energyexplained/electricity/how-electricity-is-generated.php>> [Accessed 20 April 2022]

Vetaphone, 2020. *Corona or plasma?* [online] Available at: <<https://www.vetaphone.com/corona-or-plasma/>> [Accessed 4 September 2022].

Vora-ud, A., Chaarmart, K., Kasemsin, W., Boonkirdram, S. and Seetawan, T., 2022. Transparent thermoelectric properties of copper iodide thin films. *Physica B: Condensed Matter*, 625. <https://doi.org/10.1016/j.physb.2021.413527>.

Wang, X., Suwardi, A., Lim, S.L., Wei, F. and Xu, J., 2020. Transparent flexible thin-film p–n junction thermoelectric module. *npj Flexible Electronics*, 4(1). <https://doi.org/10.1038/S41528-020-00082-9>.

*Why is glass transparent?* 2014. [YouTube] Miodownik, M. Available at: <<https://www.youtube.com/watch?v=VwRLIt6jgdM>> [Accessed 14 April 2022]

Won, P., Kim, K.K., Kim, H., Park, J.J., Ha, I., Shin, J., Jung, J., Cho, H., Kwon, J., Lee, H. and Ko, S.H., 2021. *Transparent Soft Actuators/Sensors and Camouflage Skins for Imperceptible Soft Robotics*. *Advanced Materials*, <https://doi.org/10.1002/adma.202002397>.

Wu, B., Guo, Y., Hou, C., Zhang, Q., Li, Y. and Wang, H., 2021. From carbon nanotubes to highly adaptive and flexible high-performance thermoelectric generators. *Nano Energy*, 89, p.106487. <https://doi.org/10.1016/J.NANOEN.2021.106487>.

Wu, Q., Miao, W.S., Zhang, Y. du, Gao, H.J. and Hui, D., 2020. Mechanical properties of nanomaterials: A review. *Nanotechnology Reviews*, 9(1), pp.259–273. <https://doi.org/10.1515/NTREV-2020-0021>.

Wu, X., Wang, Z., Liu, Y., Sun, X., Xu, Y., Tian, Y., Wang, B., Sang, X., Shi, J. and Xiong, R., 2022. Enhanced performance of Bi<sub>2</sub>Te<sub>3</sub>-based thermoelectric materials by incorporating Bi<sub>2</sub>Fe<sub>4</sub>O<sub>9</sub> magnetic nanoparticles. *Journal of Alloys and Compounds*, 904. <https://doi.org/10.1016/j.jallcom.2022.163933>.

Yamamoto, Y., Aramaki, T., Ito, R. and Kimura, M., 2021. GTO thin film thermoelectric conversion device manufactured by RF magnetron sputtering method. In: *2021 28th International Workshop on Active-Matrix Flatpanel Displays and Devices (AM-FPD)*. pp.102–105. <https://doi.org/10.23919/AM-FPD52126.2021.9499210>.

Yoshida, A. and Toshima, N., 2016. Thermoelectric Properties of Hybrid Thin Films of PEDOT-PSS and Silver Nanowires. *Journal of Electronic Materials*, [online] 45(6), pp.2914–2919. Available at: <<https://login.libezp2.utar.edu.my/login?url=https://search.ebscohost.com/login.aspx?direct=true&db=iih&AN=114885576&site=eds-live&scope=site>>.

Zeng, F., Zhao, X., Luo, M., Wang, W., Qing, X., Lu, Y., Zhong, W., Liu, Q., Luo, J., Li, M., Li, M. and Wang, D., 2022. A transparent PEDOT:PSS/PVA-co-PE/epoxy thermoelectric composite device with excellent flexibility and environmental stability. *Composites Science and Technology*, 218. <https://doi.org/10.1016/j.compscitech.2021.109153>.

Zheng, Z., Cao, J., Wu, W. and Leung, M.K.H., 2022. Parallel and in-series arrangements of zeotropic dual-pressure Organic Rankine Cycle (ORC) for low-grade waste heat recovery. *Energy Reports*, 8, pp.2630–2645. <https://doi.org/10.1016/J.EGYR.2022.01.057>.

## APPENDICES

### Appendix A: Gantt Chart for January 2022 Trimester

No.	Project Activities	Planned Completion Date	W1	W2	W3	W4	W5	W6	W7	W8	W9	W10	W11	W12	W13	W14	W15	W16	W17
1.	Problem formulation and project planning	2022-02-13																	
2.	Literature Review	2022-04-17																	
3.	Methodology and workplan	2022-04-22																	
4.	Introduction and report finalization	2022-04-24																	
5.	Presentation slides preparation	2022-04-24																	
6.	Progress report and presentation slides submission	2022-04-25																	

